Adsorption (2025) 31:90
https://doi.org/10.1007/s10450-025-00641-4

Analyzing the gas storage capacities of NU-2100 MOF via GCMC simulations: a material with remarkable hydrogen volumetric storage attributes

A. Granja-DelRío[1] · I. Cabria[1]

Received: 24 March 2025 / Revised: 5 June 2025 / Accepted: 8 June 2025

Abstract
Materials capable of effectively storing H_2 and CH_4 are essential for the enhancement of hydrogen and methane-based transportation. Metal-Organic Frameworks (MOFs) are strong contenders for meeting the gas storage targets of the Department of Energy (DOE). Many Cu(I)-based MOFs degrade in air and moisture. NU-2100, a newly developed Cu(I)-based MOF, shows air stability. The total and usable H_2 and CH_4 storage capacities of NU-2100 at 298.15 K and 0.5–35 MPa are calculated and analyzed by means of Grand Canonical Monte Carlo (GCMC) studies. A comparative assessment is performed, including MOFs with similar metal compositions, pore size, density and porosity at 298.15 K and 25 MPa. The findings demonstrate that NU-2100 exhibits storage capacities that match or outperform the MOFs included in this investigation. The origin of these higher capacities is that the molecules interact with the atoms of NU-2100 in wider regions or pores than in the other MOFs. The autonomy range of a hydrogen and a methane vehicle containing NU-2100 are also calculated. A hydrogen or a methane vehicle storing the gas on this new material would reach the same autonomy as a vehicle storing the gas by compression, using a larger tank volume and lower pressures.

Keywords Metal-organic frameworks · Grand Canonical Monte Carlo · Methane storage · Hydrogen storage · Cu(I)-based MOF

1 Introduction

Transportation is a fundamental element connecting people, cultures, cities, and countries. It underpins modern economies by supporting global trade and enabling travel. It also ensures access to essential services like education and healthcare, improving quality of life. However, the sector has notable downsides, including significant environmental and health impacts. It accounts for about 25% of the EU greenhouse gas emissions [1–4] and contributes to air and noise pollution as well as habitat fragmentation [5].

A transition to a carbon-free energy system by replacing fossil fuels with renewable sources is a potential solution. Hydrogen emerges as a promising green energy carrier due to its high gravimetric energy density [6–8], offering 120 MJ/kg compared to gasoline's 44 MJ/kg [9]. However, its low volumetric energy density makes large-scale storage for vehicles challenging. The key obstacle is developing onboard storage systems that provide a driving range of over 600 km per fill [10–14]. Currently, hydrogen is stored as a compressed gas at pressures up to 70 MPa [15], which raises concerns regarding safety and cost.

There are specific storage targets issued by the U.S. Department of Energy (DOE), for the year 2025: At least 0.040 kg H_2/L and 5.5 wt% for the volumetric and gravimetric capacities [9, 16]. These targets refer to hydrogen usable, deliverable or working capacities for vehicle range and focus on reversible storage for repeated refilling and release. Hydrogen vehicles aim for zero greenhouse gas (GHG) emissions, but interim solutions may be needed. Natural gas, mainly composed by CH_4, offers a lower-emission bridge due to its availability, infrastructure, and cost [17]. With a high H/C ratio, it can cut CO_2 emissions by about 55%, aligning with EU targets [18]. Hence, natural

✉ I. Cabria
ivan.cabria@uva.es

[1] Departamento de Física Teórica, Atómica y Óptica, Universidad de Valladolid, 47011 Valladolid, Spain

Published online: 14 July 2025

gas is an attractive option for mitigating environmental impacts [19–22].

Methane has a low volumetric but high gravimetric capacity at ambient conditions. Currently, vehicles store it by compression at 25–35 MPa. Using solid porous materials for storage can lower pressure and reduce costs [23, 24]. To guide research efforts, the Advanced Research Projects Agency-Energy (ARPA-E) outlined methane storage targets. These targets include achieving volumetric and gravimetric capacities of 0.250 kg of CH_4 per liter and 33.33 wt%, respectively, at room temperature and moderate pressures [23–27].

Adsorbed gas storage offers an alternative to compression and liquefaction, using porous solids to hold CH_4 or H_2 at pressures equal or below 25–35 MPa. Lowering the pressure enables lighter, cheaper, and more conformable tanks [27, 28]. Researchers have delved into various categories of solid porous materials with applications on gas storage [29–51].

Metal-organic frameworks (MOFs) have enhanced gas storage by allowing tunable properties [52–54]. MOFs have total hydrogen volumetric and gravimetric capacities within the intervals 0.0005–0.0150 kg/L and 0.3–2.3 wt%, respectively, at room temperature and pressures between 5 and 10 MPa [55]. IRMOF-1 (Isoreticular MOF), a well-known material also referred to as MOF-5, has a total hydrogen gravimetric capacity of 0.45 wt% at 298 K and 6 MPa [56]. As regards methane storage, the total volumetric and gravimetric capacities of MOFs are within the intervals 0.0072–0.2146 kg/L and 2.9–23 wt% at room temperature K and 3.5–6.5 MPa [23, 43, 57–61]. The total volumetric and gravimetric methane capacities of IRMOF-1 at 3.6 MPa and 300 K are 0.0787 kg/L and 13.5 wt%, respectively [62]. HKUST-1, another MOF, has total volumetric and gravimetric capacities of 0.1910 kg/L and 17.8 wt%, respectively at 298 K and 6.5 MPa [43]. Yet, storing large H_2 amounts at ambient conditions remains difficult due to the extremely small polarizability of the H_2 molecule [63, 64]. MOFs with open metal sites enhance gas adsorption by acting as strong Lewis acids. These materials improve storage at mild temperatures [49, 50, 65–76]. Research has been conducted on the adsorption capabilities of MOFs, including their capacity to store methane and hydrogen. This exploration has been carried out through many experimental [70, 77–84] and computational studies [81, 85–95]. Among the simulation methods employed, the Grand Canonical Monte Carlo (GCMC) method has been widely utilized [30, 32, 33, 81, 96–98].

Recent research has showcased Cu(I)-based MOFs as having notably high hydrogen isosteric heats, but often degrade in air and moisture. Consequently, research focuses on creating stable versions for hydrogen storage. A research team from Northwestern University (NU) [99] has developed NU-2100, a Cu(I)-based MOF with air stability, and measured its hydrogen storage capacities at 273 and 296 K and up to 10 MPa. This MOF was synthesized utilizing a blend of Cu/Zn precursors. NU-2100 exhibits air-stability and demonstrates a high isosteric heat (32 kJ/mol, 0.332 eV) alongside favorable hydrogen storage capabilities at ambient conditions: A volumetric capacity of 0.0105 and 0.0075 kg/L at 296 and 273 K, respectively, and 10 MPa [99].

The present study aims to assess the potential of NU-2100 as a storage material by determining its usable H_2 and CH_4 capacities at 298.15 K. GCMC computational simulations were performed to compute the storage capacities of the newly synthesized NU-2100 for the pressure interval 0.5–35 MPa under room temperature conditions. To delve deeper into the characteristics of the newly synthesized NU-2100 MOF Cu-based, which posses an equivalent number of C and N, GCMC computational simulations were performed to assess the capacities of Cu-based MOFs with identical or comparable C/metal and N/metal ratios as NU-2100. The capacities of NU-2100 and the selected Cu-based MOFs were then analyzed. Additionally, the MOFs with similar porosity and density as NU-2100 were chosen to compare their capacities with those of NU-2100 MOF.

Moreover, the correlation between the structural properties (pore size, density and porosity) and the capacities of the simulated MOFs was investigated. This exploration into the interactions between MOFs and adsorbed molecules is crucial for comprehending the origins of the capacities and designing novel MOFs. Unless specified otherwise, the term ‘capacities’ means usable storage capacities, throughout this paper.

2 Methodology

2.1 Parameters and details of the simulations

GCMC simulations were conducted at pressures in the interval 0.5–35 MPa and at 298.15 K, and were employed to generate the isotherms of methane and hydrogen for NU-2100 MOF [80]. A single GCMC simulation lasted ten million iterations. To guarantee equilibrium, half of these iterations, the first five million, were allocated to the equilibration phase. The last five million iterations were employed to compute the gas storage capacities.

In every iteration, the Metropolis algorithm [100] was applied. An in-house software called mcmgs was used to run the simulations. The source files of this code, the instructions to compile and run the code and examples of input and output files can be found at the GitHub platform [101]. Adjustments or movements such as molecule insertion,

deletion, and translation were implemented, adhering to the proportions outlined by Granja-DelRío et al. in reference [102]. The chemical potential was computed from the Soave-Redlich-Kwong equation of state (SRK EOS) [103]. The parameters of the SRK EOS for H_2 and CH_4 are those in references [104] and [105], respectively.

The atoms of the simulation cells were kept fixed during the simulations. Only the hydrogen or methane molecules could be translated on an iteration. A molecule is considered as a single point and it does not have dipole nor multipoles. The simulation cell is replicated in the three spatial directions. In every iteration, the molecules of the simulation cell interact with the atoms and molecules of the simulation cell and also with the atoms and molecules of the 26 nearest neighbour replicated cells in the three spatial directions.

The Lennard-Jones (LJ) potentials [106] were harnessed to simulate the atom-molecule and molecule-molecule interactions. The Lennard-Jones potential, a well-established representation, encapsulates the repulsive and attractive aspects of the interactions. The LJ parameters, σ and ϵ, depend on the atoms and molecules involved in the interaction and are implemented as in Granja-DelRío et al. work [102]. The LJ parameters used in the simulations are in Table S1 in the Supporting Information. The predefined cutoff radii of H_2 and CH_4 dictating the LJ interaction potential were extensively outlined in previous studies [31, 32]. An alternative set of Lennard-Jones (LJ) coefficients, known as the MDT set (from Mayo, Darkrim, and TraPPE), was chosen to enable a comparison between different interaction potentials (see Fig. 1). In the MDT set, LJ parameters for atoms are taken from Mayo et al. [107], those for hydrogen from Darkrim and Levesque [108], and those for methane from the TraPPE model [109]. These coefficients can be found in Table S2. Figure S2 shows that, in the case of hydrogen, there is a slight difference between the sets, and the MDT coefficients may slightly overestimate the adsorption capacity. On the other hand, for methane, both sets of coefficients give almost the same results, with no noticeable difference. The Feynman-Hibbs correction was considered to incorporate quantum effects into the interaction potential [110], which was uniformly applied across all GCMC simulations. The electrostatic interactions are not included. We have tested this GCMC model vs experimental results of pure or bulk gases (H_2 and CH_4) [31, 32] and vs experimental storage capacities of different materials [30, 102, 111].

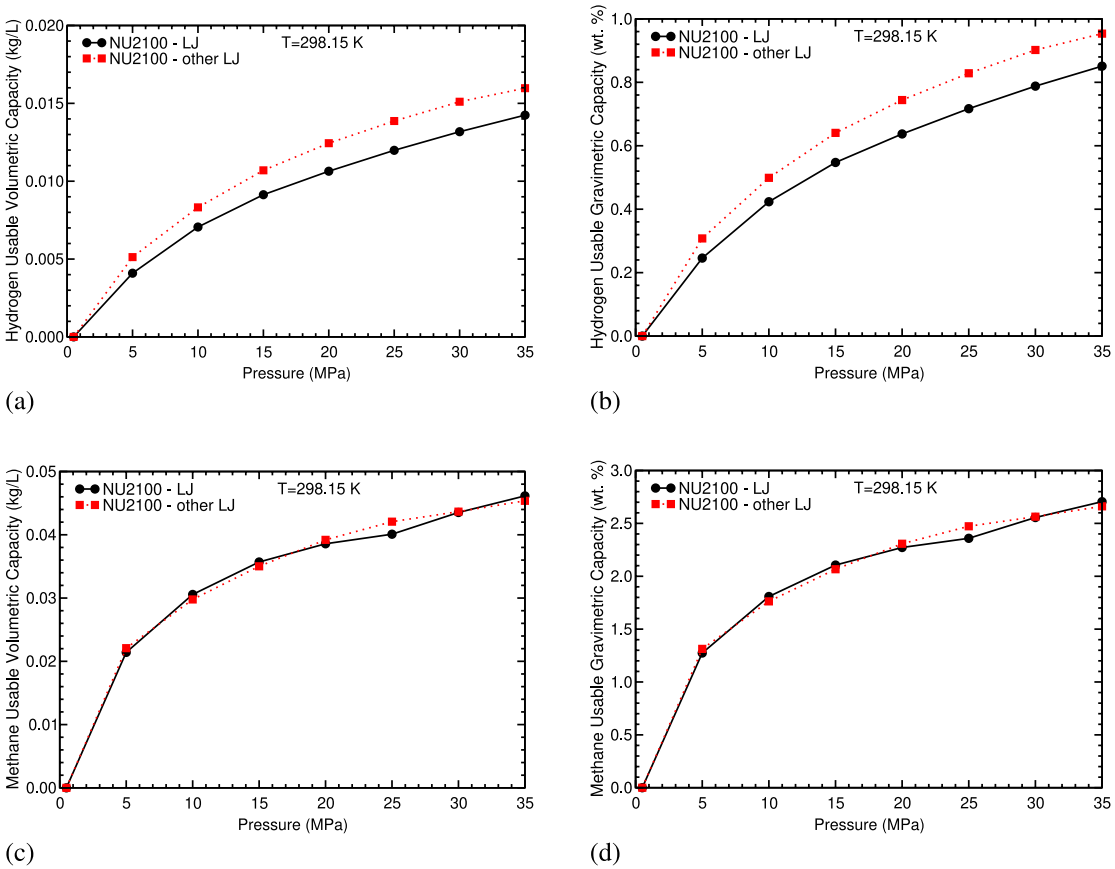

Fig. 1 Hydrogen usable storage capacities at 298.15 K vs pressure (panels (**a**) and (**b**)) and methane usable storage capacities at 298.15 K vs pressure (panels (**c**) and (**d**)) for NU-2100

The isosteric heats and the usable volumetric and gravimetric storage capacities were computed based on the published definitions [31, 102]. The pore radii and porosity of the materials was calculated using a procedure previously published [31]. The porosity and pore radii for H_2 and CH_4 are, in general, different.

2.2 Simulation cells and sets of MOFs

To thoroughly evaluate the storage capacities, GCMC simulations were conducted on NU-2100, a Cu-based MOF [80] and on three distinct groups of MOFs. These groups include: (a) a group of Copper-based MOFs with Carbon/Copper ratios identical to the ratio of NU-2100, 3.0, (b) a group of Copper-based MOFs with Nitrogen/Copper ratios identical to the Nitrogen/Copper ratio of NU-2100, 3.0, and c) a group of MOFs with porosity-density ($P-\rho-$) properties akin to those of NU-2100.

The Crystallographic Database Center (CCDC) repository provides Crystallographic Information File (CIF) data [112]. The NU-2100 simulation cell [80] was retrieved from the general CCDC repository, while the simulation cells for the other MOFs were obtained from the MOF CCDC subset [113]. The MOF names are the identifiers of the MOFs in the CCDC repository. The simulation cell of NU-2100 is showcased in Fig. 2, employing the grace software for visualization [114].

The Copper-based set of MOFs with Carbon/Copper ratio equal to NU-2100's ratio of 3.0 was selected from the CCDC database. These MOFs are AYONOT, FAQSOG, GUSPUG, JOFKIA, JOFKIA01, MACUFR02, NURSIF, QOXNEX and WUZDOL for hydrogen and methane analysis. Seven Cu-based MOFs with Nitrogen/Copper ratios matching NU-2100's 3.0 ratio were selected from the CCDC database. These MOFs, chosen for hydrogen and methane analysis, are FOQJAA (also called Cu-DCBBT-MOF), FIRTIL, NELWIL, RORSID01, RORSID02, RORSID03, RORSID04, RORSID05, RORSID06, RORVOM, RORVUS and RORVUS01.

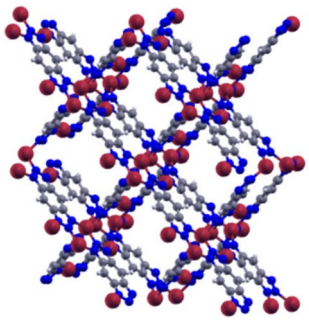

Fig. 2 The cell of NU-2100 used in the simulations. Cu, N, H and C atoms are depicted by red, blue, white and gray spheres, respectively. Colour figure online.

The MOFs in the P-ρ group were selected from the CCDC database, targeting MOFs with porosity for hydrogen within approximately 23% and density within 8% of NU-2100. This selection forms the $P-\rho-$ set, and the CCDC database identifiers for these MOFs are ATIBOU, AZAFIS, LETROT, NIHBIQ01, QUTTII, QUZVEO, VIWKOD, VOSWAE, WEMDUP, XIFHIF and YEMJAC. For methane, the selection targeted MOFs with porosity within approximately 15% and density within 8% of NU-2100, consisting of the same MOFs as the hydrogen case plus YUPSIM. The details of the simulation cells of all the MOFs studied can be found in Table S3 in the Supporting Information.

GCMC simulations were conducted for each MOF within the designated sets, alongside NU-2100, employing identical temperature, pressure, and simulation parameters as previously described. This systematic approach enables a comprehensive analysis and direct comparison of their capacities.

2.3 Assessment of the Feynman-Hibbs correction in gas adsorption simulations

Figure 3 shows the results of the simulations with and without the Feynman-Hibbs (FH) correction at 298.15 K and pressures between 0 and 35 MPa. As we can see in the graphs, the total hydrogen adsorption capacities are very similar in both cases, with and without the FH correction. However, a small difference can be observed, which increases slightly with pressure, where the FH correction results in slightly lower values. Although the effect of the correction is not very significant under these temperature and pressure conditions, we decided to apply it in all our GCMC simulations. This choice helps maintain consistency throughout the study and will also be useful for future research at lower temperatures, such as 77 K, where quantum effects are more relevant and the FH correction becomes more important.

Figure 4 presents the simulation results for methane adsorption with and without the Feynman-Hibbs correction at 298.15 K and pressures from 0 to 35 MPa. The graphs show that the total adsorption capacities are almost the same in both cases. On the other hand, there is a small difference in the usable capacities: the values are slightly lower when the correction is applied. Similar to what was observed with hydrogen, the impact of the correction is quite small at this temperature and pressure range.

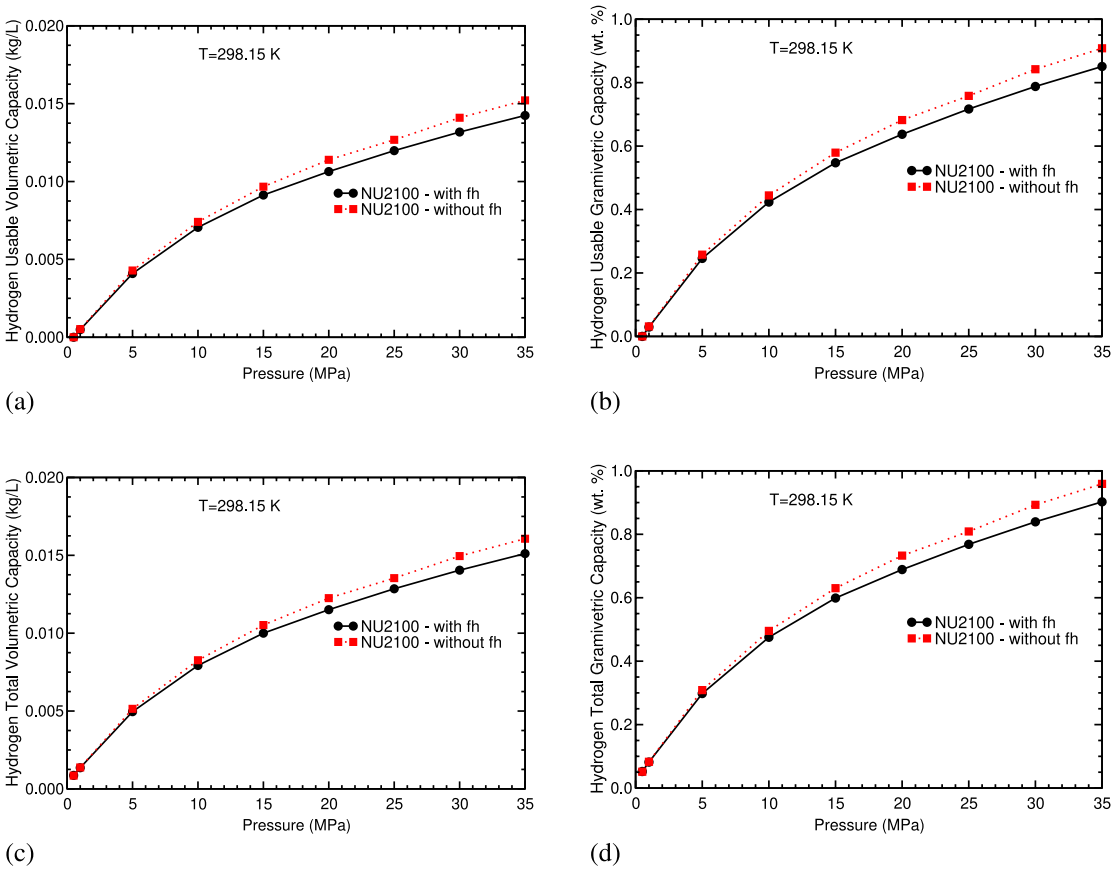

Fig. 3 Hydrogen usable storage capacities at 298.15 K vs pressure (panels (**a**) and (**b**)) and hydrogen total storage capacities at 298.15 K vs pressure (panels (**c**) and (**d**)) for NU-2100

3 Analysis of the hydrogen usable storage capacities

3.1 Comparison of experimental and GCMC hydrogen capacities of NU-2100

The team from the Northwestern University (NU) [99] published also the total hydrogen storage capacities at 273 and 296 K, near the room temperature of 298.15 K, obtained in their experiments up to 10 MPa. GCMC simulations of the total hydrogen storage capacities of NU-2100 have been also performed in the present study at those temperatures and pressures up to 10 MPa, to compare the GCMC results with the experiments. The comparison is shown in Fig. 5. The agreement between the experimental and the present GCMC total capacities is reasonable: The relative difference between the experimental and the GCMC gravimetric capacities is within the range 2–11% and the relative difference between the volumetric capacities falls within the range 7–19%. Hence, the present GCMC gravimetric and volumetric capacities have relative errors equal to the above mentioned relative differences.

3.2 Dependence on the structural parameters

GCMC simulations performed at 25 MPa and 298.15 K yielded data on the usable capacities for NU-2100 and the MOFs of the C/Cu, N/Cu and P-ρ-based sets. Figures 6, 7, 8 present these results, showing the relationships between these capacities and parameters such as porosity, density, pore radii, isosteric heat and the product of porosity and isosteric heat.

As showed in Fig. 6, the capacities diminish with increasing material density and rise with increasing porosity. These general trends have also been found in different types of MOFs, not only in the present studied MOFs, and carbon nanostructures [30–32, 102, 111, 115]. While most MOFs adhere to these patterns, there are some exceptions. Moreover, it is evident from Fig. 6 that the gravimetric capacity of NU-2100 matches the trend observed in C/Cu, N/Cu and $P-\rho-$based MOFs, i.e., the gravimetric capacity of NU-2100 is similar to the gravimetric capacity of MOFs with similar densities and porosities. However, it is noteworthy that NU-2100 exhibits significantly higher volumetric capacity compared to the volumetric capacities of other MOFs with similar densities and porosities. This implies the

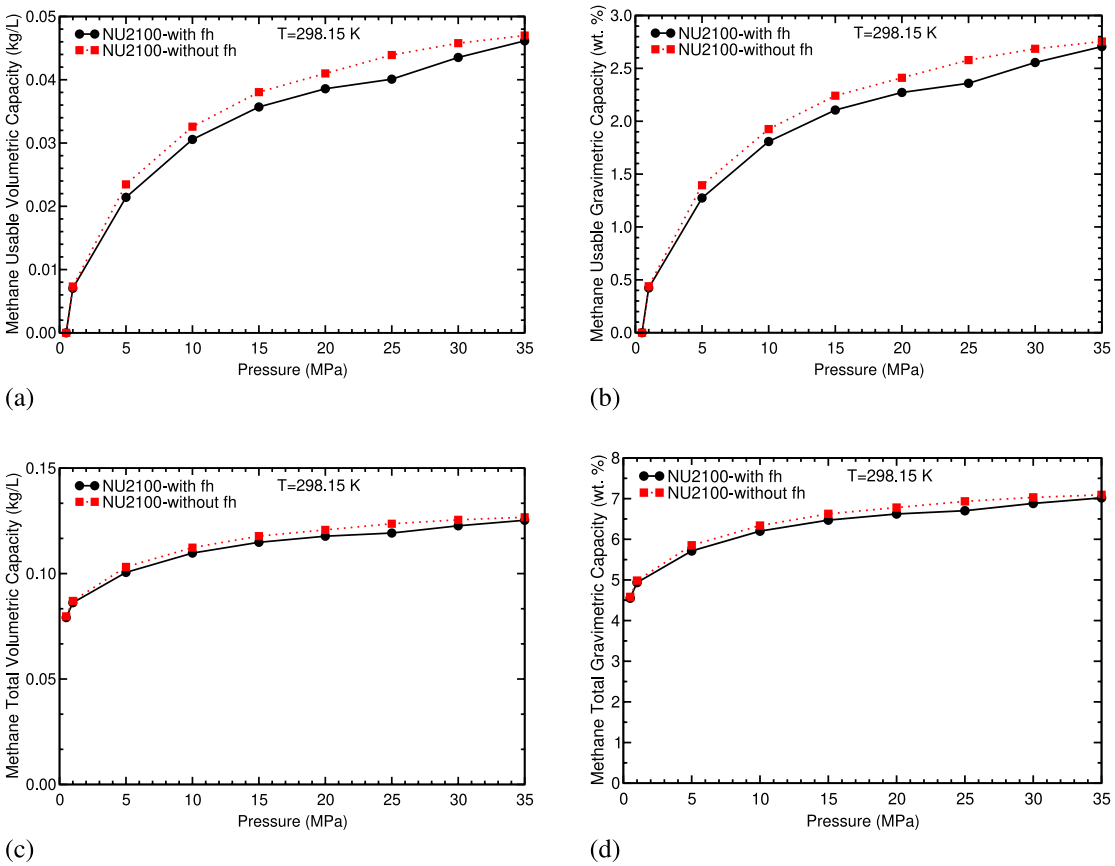

Fig. 4 Methane usable storage capacities at 298.15 K vs pressure (panels (**a**) and (**b**)) and methane total storage capacities at 298.15 K vs pressure (panels (**c**) and (**d**)) for NU-2100

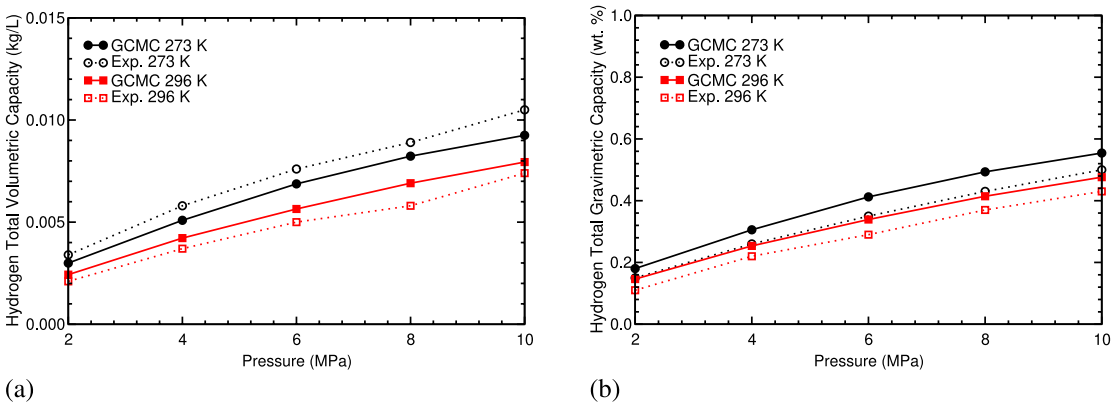

Fig. 5 Hydrogen total volumetric in kg/L (**a**) and gravimetric in wt% (**b**) capacities of NU-2100 obtained in the experiments [99] and in the current GCMC simulations at 273 and 296 K and at different pressures.

potential to forecast NU-2100's usable gravimetric capacity using either its porosity or density as predictors.

The pore radii-capacities correlation is depicted in Fig. 7 for NU-2100 and related MOFs. The gravimetric capacity shows a consistent linear growth as the pore radius, average and largest, increases. It's essential to acknowledge that, generally, a pore radius increase correlates with a density reduction, which results into a higher gravimetric capacity. This trend represents a rough estimate.

An initial expansion of the pore radius leads to a boost in the volumetric storage capacity. Beyond a certain value, there is a saturation phenomenon, reaching the volumetric capacity a constant value as the radius of the pore increases.

The best-performing MOFs from the C/Cu, N/Cu and $P-\rho-$based sets were selected for analysis and listed in

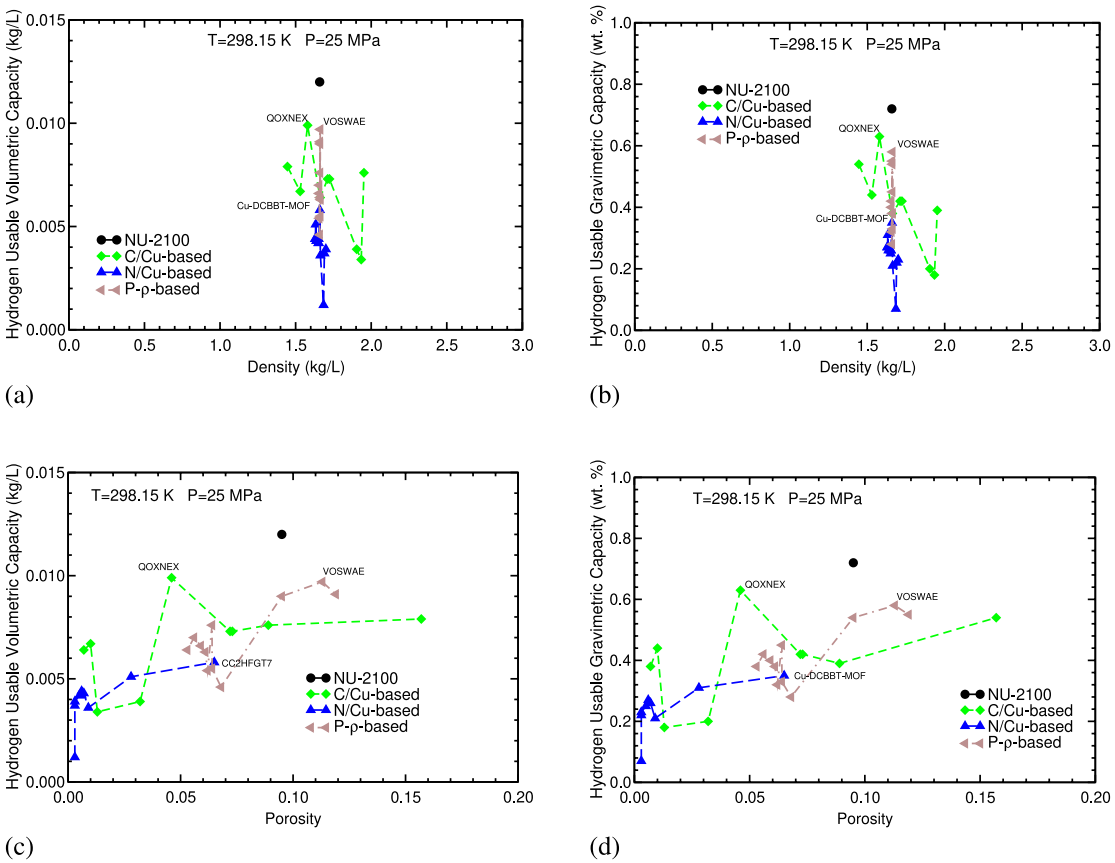

Fig. 6 Hydrogen usable storage capacities at 25 MPa and 298.15 K vs density (panels (**a**) and (**b**)) and porosity (panels (**c**) and (**d**)) for NU-2100, C/Cu, N/Cu and $P-\rho$−based MOFs.

Table S4. These include QOXNEX [116, 117] from the C/Cu-based group (see Fig. S1), Cu-DCBBT-MOF [118, 119] from the N/Cu-based group, which is reported as a material for selective adsorption and gas separation, and VOSWAE [120] from the $P-\rho$−based group (see Fig. S1). The comparison of NU-2100 with the other sets of MOFs indicates that NU-2100 has higher volumetric capacities. Tables S4 contain the storage capacities and the main structural properties of these selected MOFs.

Gas adsorption and storage are inherently connected to the isosteric heat, Q_{st}, representing the bond strength between the adsorbent material and a gas molecule. Therefore, it is logical to examine the correlation between isosteric heat and storage capacities.

The capacities of the selected MOFs and NU-2100, alongside Q_{st} and the product of the porosity and Q_{st}, have been depicted in Fig. 8. The isosteric heats for the studied porous materials range from 0.06 to 0.11 eV. Furthermore, the product of porosity and isosteric heat falls within the range of 0.00 to 0.01 eV.

With increasing isosteric heat, there is a tendency for the gravimetric capacity to decrease, although the trend is not consistent. The volumetric capacity does not exhibit a clear pattern. However, both capacities generally increase with higher values of the isosteric heat multiplied by porosity. The relationship of both capacities with the product of porosity and Q_{st} is non-monotonic, exhibiting numerous oscillations around an average trend. The dependence of the volumetric capacity on the product of the porosity by Q_{st} is nearly linear. Hence, increasing that product, materials with high volumetric capacity could be discovered.

3.3 Dependence on the pressure

The total and usable storage capacities of NU-2100 and the MOFs with the highest capacities among the selected groups, including a well-known and benchmark material such as IRMOF-1, are plotted vs the pressure in Fig. 9 at 298.15 K. These are also called the isotherms, in this case the hydrogen isotherms. There are experimental hydrogen storage capacities of NU-2100 at 296 K up to 10 MPa. Hence, the hydrogen storage capacities of NU-2100 on that figure at 298.15 K and 10–35 MPa are predictions for future experiments on NU-2100 at those conditions.

NU-2100 exhibits higher total and usable capacities than the best MOFs of the C/Cu, N/Cu and P-ρ-based sets. At

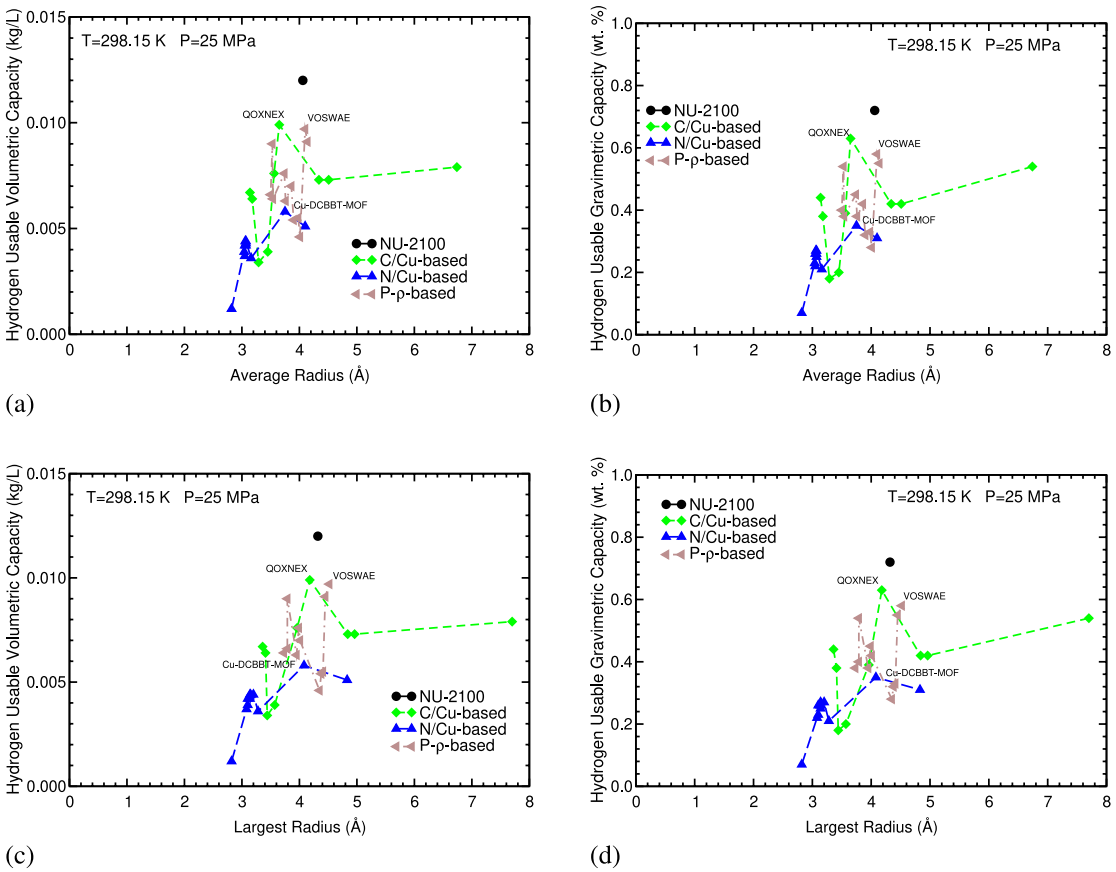

Fig. 7 Hydrogen usable storage capacities at 25 MPa and 298.15 K vs average pore radius (panels (**a**) and (**b**)) and largest pore radius (panels (**c**) and (**d**)) for NU-2100, C/Cu, N/Cu and $P-\rho-$based MOFs.

35 MPa, NU-2100 notably achieved 0.014 kg/L, the highest usable volumetric capacity, which is approximately 35% of the DOE volumetric capacity target [9, 16].

To better evaluate the potential of the selected MOFs, IRMOF-1 was included in the comparison as a classical and widely studied material. NU-2100 outperforms IRMOF-1 in both total and usable volumetric capacities at pressures up to 15 MPa. At higher pressures, however, IRMOF-1 shows slightly higher volumetric capacities It shows higher gravimetric capacities above 15 MPa, because the density of IRMOF-1 is about 2.8 times lower than the density of NU-2100 (See Table S4).

The NU-2100, QOXNEX, Cu-DCBBT-MOF and VOSWAE hydrogen isotherms saturate at approximately the same high pressures, which is consistent with the fact that these MOFs have approximately the same largest and average pore radius (See Table S4). The total capacities of the five MOFs (see Fig. 9) have similar values at 0.5 MPa. Hence, the usable hydrogen isotherms of the five MOFs resemble the total hydrogen isotherms.

The total and usable isotherms of QOXNEX and VOSWAE closely resemble those of NU-2100 and are about 10% smaller. Conversely, the isotherms of Cu-DCBBT-MOF exhibits values approximately 50% lower than those of NU-2100. The four MOFs, NU-2100, QOXNEX, Cu-DCBBT-MOF and VOSWAE, have similar porosity, density and pore radii. Usually, MOFs with similar porosity-density-pore size properties have also similar storage capacities. NU-2100 and Cu-DCBBT-MOF do not fall within that general trend. Hence, those structural parameters can not be used as the only reason to explain the isotherms of NU-2100 and Cu-DCBBT-MOF. NU-2100 and QOXNEX have the same C/Cu ratio, 3.00. However, Cu-DCBBT-MOF, the best MOF of the N/Cu-based set, has a very different C/Cu ratio, 15.00. In fact, all the MOFs of the N/Cu-based set, which they have N/Cu = 3.00, have C/Cu ratios between 7 and 15.

To further inquiry in the origins of the difference among the isotherms of the studied MOFs, we have also examined the interaction potential energy of a single H_2 molecule interacting with these MOFs. That energy depends on the point (x,y,z) where the H_2 molecule is located. The 3D interaction potential energy, $V(x, y, z)$, of the MOFs are plotted in Fig. 10. The regions where the interaction potential energy is equal or smaller than 0.1 eV have been plotted in

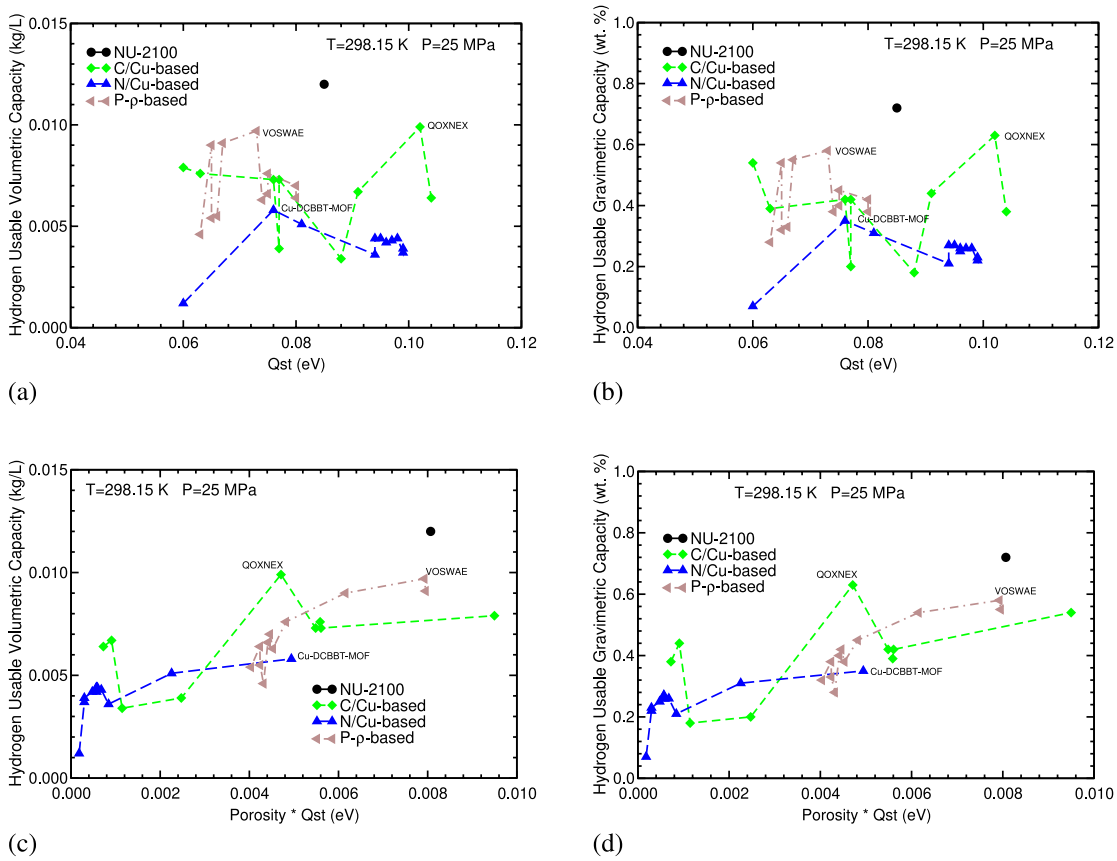

Fig. 8 Hydrogen usable storage capacities at 25 MPa and 298.15 K vs the isosteric heat (panels (**a**) and (**b**)) and vs the product of the porosity and isosteric heat (panels (**c**) and (**d**)), for NU-2100, C/Cu, N/Cu and P-ρ-based MOFs.

the left panels of that figure. The right panels in Fig.10 show the interaction potential energy at $z = 12$ Å for Cu-DCBBT-MOF and NU-2100. For IRMOF-1, the corresponding panel on Fig. 10 shows the interaction potential energy at $z = 4.25$ Å. On those z planes, the interaction potential energy of the corresponding MOF reaches its lowest value: − 0.094, − 0.072 and − 0.046 eV/molecule, for NU-2100, Cu-DCBBT-MOF and IRMOF-1, respectively. This was the reason to select and plot the energies on those planes.

The blue and black channels or pores on that figure correspond to regions where the interaction between a hydrogen molecule and the MOF is more intense. These pores do not coincide necessarily with the geometric pores. It can be noticed in Fig. 10 that the pores or channels on NU-2100 where the molecules interact strongly with the atoms of NU-2100 are wider than the corresponding channels on Cu-DCBBT-MOF. It is also important to notice that the channels on NU-2100 are approximately cylindrical and wide, while those of Cu-DCBBT-MOF are not cylindrical and are not wide. The shape of the channels or pores of Cu-DCBBT-MOF is such that it is more difficult to store molecules on Cu-DCBBT-MOF than on the channels of NU-2100 (see Figs. 2, S1 and 10). These differences on the interaction potential energies of these two MOFs explain their different capacities: The shape and width of the pores of NU-2100 allow to store more molecules than the shape and width of the pores of Cu-DCBBT-MOF, and hence, NU-2100 has larger capacities than Cu-DCBBT-MOF, in spite that the two MOFs have similar densities, porosities and pore radii.

The lowest $V(x, y, z)$ value of IRMOF-1 is higher than the lowest values of the other MOFs. This implies that IRMOF-1 interacts less strongly with the hydrogen molecules. However, IRMOF-1 shows higher storage capacities, because the pores or channels in IRMOF-1 are wider than those of NU-2100 and Cu-DCBBT-MOF, as shown in Fig. 10.

The different C/Cu ratio and the analysis of the 3D interaction potential energy $V(x, y, z)$ indicates that the porosity, density and pore radii are not the only variables or structural parameters that must be considered to understand the origin of the storage capacities of solid porous materials.

3.4 Autonomy of the hydrogen vehicle

Usually the gas is stored by compression in deposits: Compressed Gas, CG, deposits. The gas can be also stored by

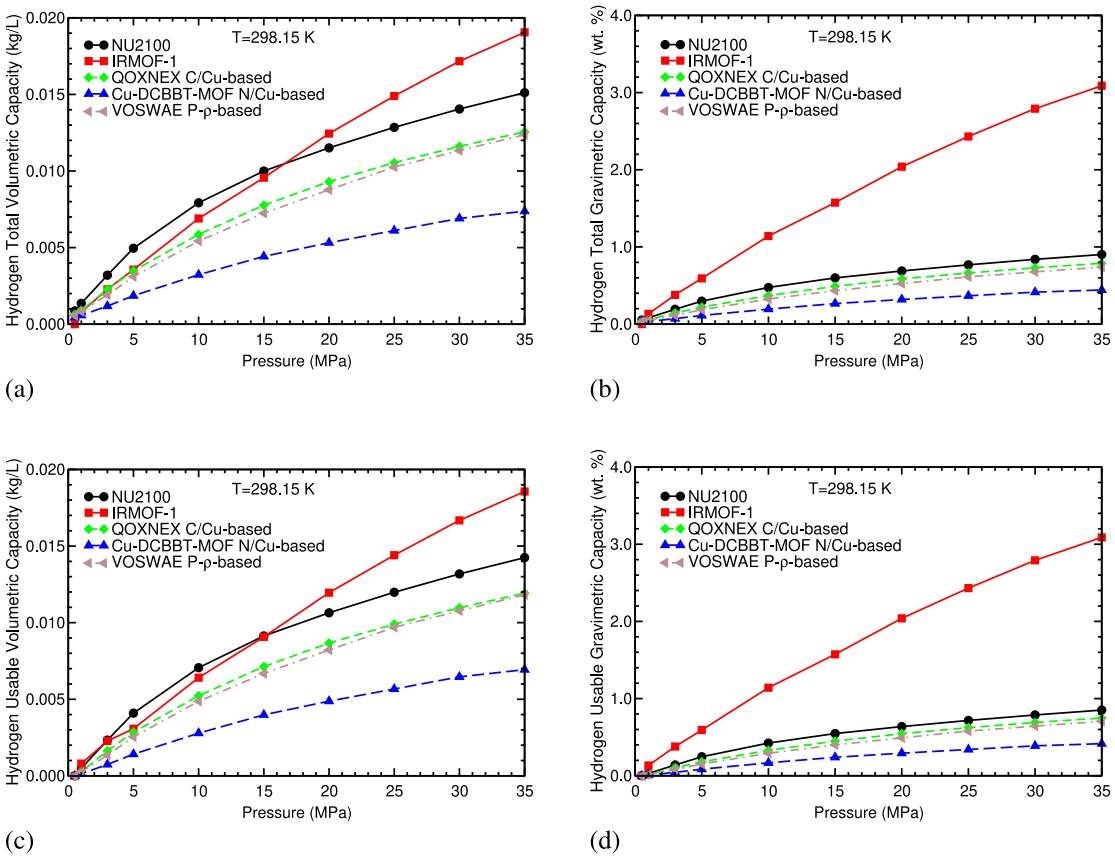

Fig. 9 Hydrogen total panels (**a**) and (**b**)) and usable panels (**c**) and (**d**)) storage capacities in relation to pressure at ambient temperature for NU-2100 and leading C/Cu, N/Cu and $P-\rho$—based MOFs and IRMOF-1.

adsorption on solid porous materials. These materials are then used inside gas deposits. These are Adsorbed Gas, AG, deposits. Besides of the calculation of the usable storage capacities of the NU-2100, the autonomy range of AG deposits with these new solid porous material have been also calculated. The autonomy is the usable volumetric capacity multiplied by the deposits volume and the fuel consumption. The number of kilometers covered using one kg of gas is the fuel consumption in km/kg units.

The 2024 Toyota Mirai is a fuel cell vehicle that stores hydrogen gas by compression [121]. The deposits volume is 142 L and store 5.6 kg of hydrogen at 70 MPa. The autonomy range of this vehicle is 402 miles (647 km approximately). The fuel consumption of the 2024 Toyota Mirai is 647 km/5.6 kg. Let's suppose that NU-2100 is used inside the deposits and that the total volume is 426 L. The hydrogen gas is stored on NU-2100. The autonomy range of that vehicle as a function of the pressure is shown in Fig. 11. The autonomy range at pressure P and 298.15 K is the usable v_c(P) of NU-2100 multiplied by the Toyota fuel consumption and 426 L. It can be noticed that the autonomy range is close to 647 km at 30 MPa and room temperature.

The autonomy of a vehicle with NU-2100 has been compared in Fig. 11 with the autonomy of a vehicle with Ni-MOF-74, a benchmark MOF with high capacities [122–125]. Both vehicles have the same deposits volume and fuel consumption. The usable capacities of Ni-MOF-74 were obtained through GCMC simulations at 298.15 K using the same in-house software, mcmgs, and then, they were used to calculate the autonomy of the Ni-MOF-74 vehicle. The two vehicles have approximately the same autonomy up to 15 MPa. For larger pressures, the Ni-MOF-74 vehicle has an autonomy a little larger. It must be considered that Al-based MOFs, such as NU-2100, are thermally stable and cheaper to synthesize than Ni-based MOFs.

4 Analysis of the methane usable storage capacities

4.1 Dependence on the structural parameters

An exploration into the methane capacities was conducted. The correlation between the structural parameters and the capacities of the MOFs has been graphically represented in

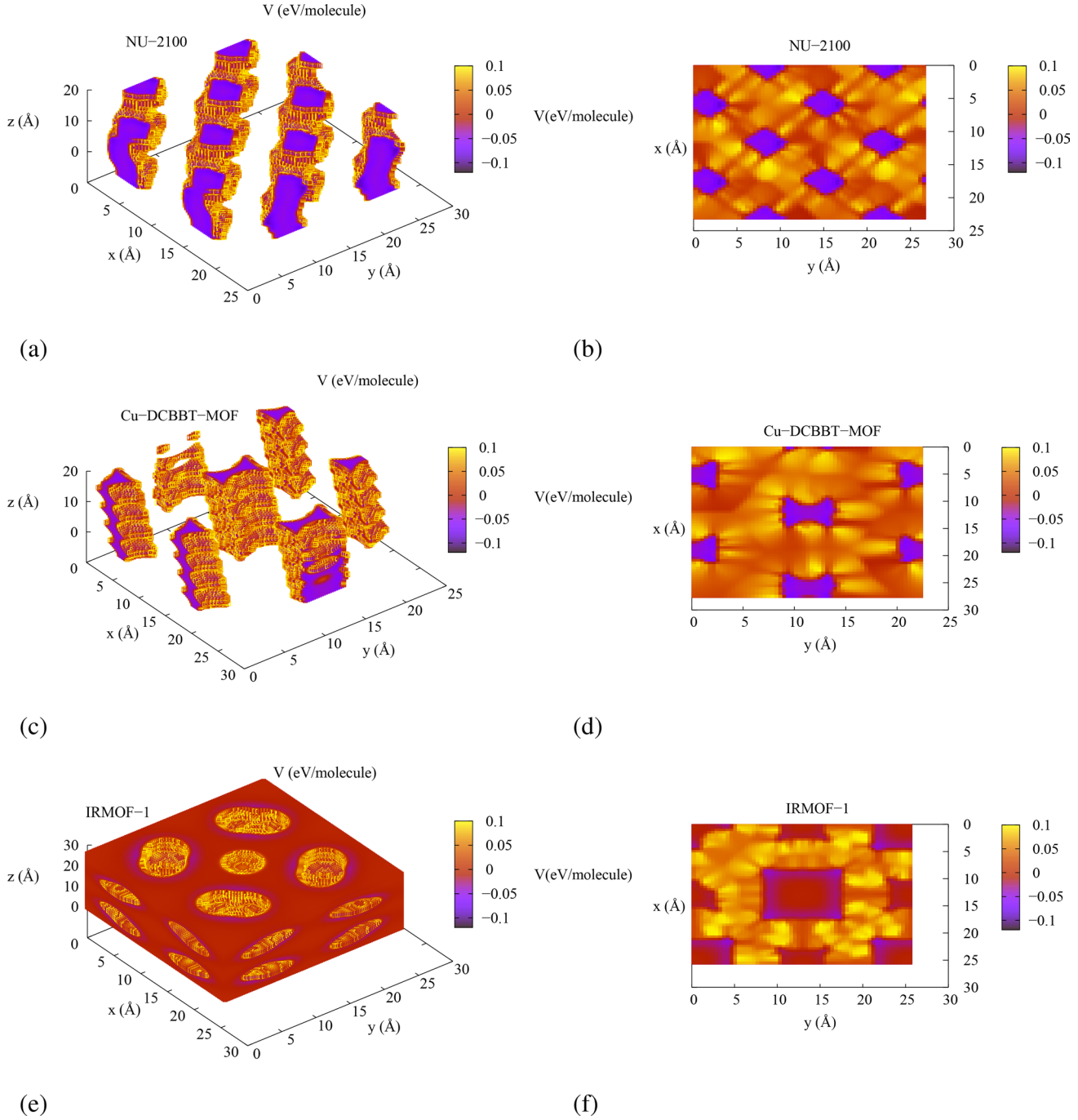

Fig. 10 Interaction potential energy in eV/molecule of a hydrogen molecule with NU-2100 (panels (**a**) and (**b**)), Cu-DCBBT-MOF (panels (**c**) and (**d**)) and IRMOF-1 (panels (**e**) and (**f**)), obtained in the present GCMC simulations

Figs. 12, 13, 14. The relationships between CH_4 capacities and density and porosity show resemblances to the relationships observed for hydrogen capacities (see Fig. 12): The capacities increase with porosity and decrease as the density increases. The NU-2100 usable capacities align with the trend of the usable capacities concerning density for the C/Cu, N/Cu and $P-\rho-$based MOFs. Nevertheless, concerning hydrogen, NU-2100 demonstrates superior volumetric capacities in relation to both porosity and density compared to its methane counterparts among the other groups of MOFs. This observation suggests that NU-2100 is more adept at storing hydrogen than methane.

The correlation between methane capacities and pore radii is depicted in Fig. 13. The capacities display a similar pattern to that observed with H_2 capacities. The capacities

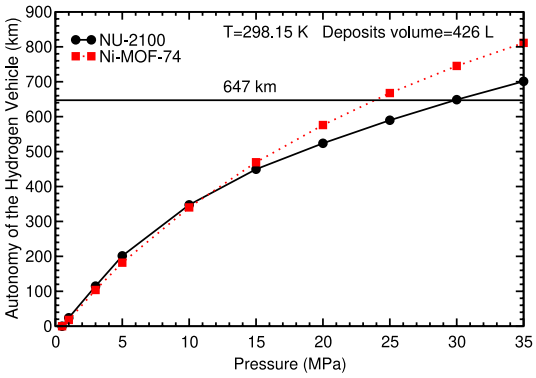

Fig. 11 Autonomy range of the hydrogen vehicle with an adsorbed gas tank containing NU-2100 vs pressure at 298.15 K

increase, in general, as the pore radius increases. The dependence on the average pore radius is not so clear.

As with the hydrogen storage analysis, the C/Cu, N/Cu and $P-\rho-$based MOFs exhibiting the highest capacities were selected for comparison with NU-2100. The selected MOFs are GUSPUG [126, 127] from the C/Cu-based group, Cu-DCBBT-MOF from the N/Cu-based group and WEMDUP [128, 129] from the $P-\rho-$based group. The methane capacities, pore radii, porosities, densities and C/metal ratios of these selected MOFs are detailed in Table S4. QOXNEX exhibits the greatest hydrogen storage capacities in both gravimetric and volumetric terms within the C/Cu-based set. For methane storage, however, GUSPUG shows the highest gravimetric and volumetric capacities. As regards the $P-\rho-$based group, VOSWAE and WEMDUP have the highest hydrogen and methane capacities, respectively.

The usable hydrogen capacities of NU-2100 are higher than the capacities of the MOFs of the C/Cu, N/Cu and $P-\rho-$based groups. However, its usable methane capacities are in the middle of the usable capacities of the C/Cu, N/Cu and $P-\rho-$based groups. The origin of this difference is that the pores of NU-2100 are narrow for methane. The size of the pores of NU-2100 could be wide enough for hydrogen, but not wide enough for methane, which is a much larger molecule. These facts can be noticed in Table S4 and Fig. 13: The MOFs with high volumetric methane capacities correspond to R_l of 8–12 Å. NU-2100 has a R_l of 4.3 Å and hence, it has a low methane usable capacity.

The dependence of the methane capacities on the isosteric heat, shown in Fig. 14, does not follow a clear trend. The product of the porosity and isosteric heat is a combination of two major influences on the storage capacities:

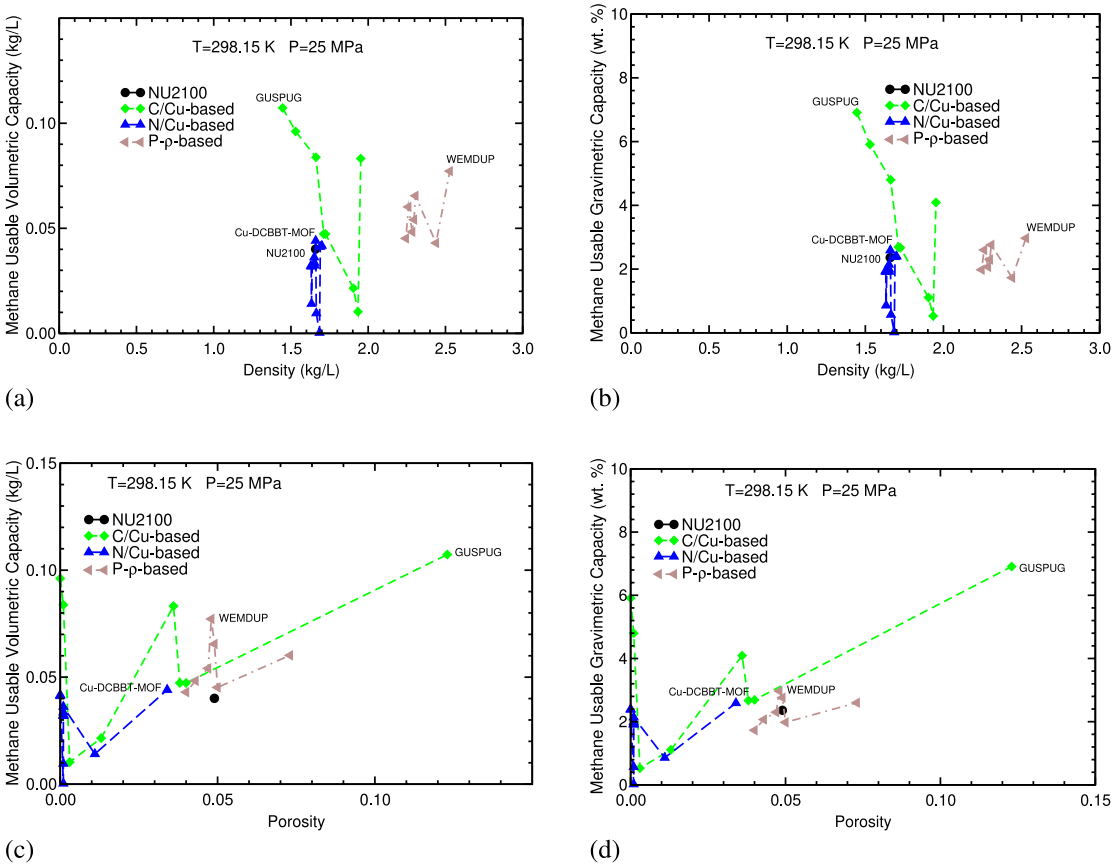

Fig. 12 Methane usable storage capacities at 25 MPa and 298.15 K vs density (panels (**a**) and (**b**)) and porosity (panels (**c**) and (**d**)), for NU-2100, C/Cu, N/Cu and P-ρ-based MOFs.

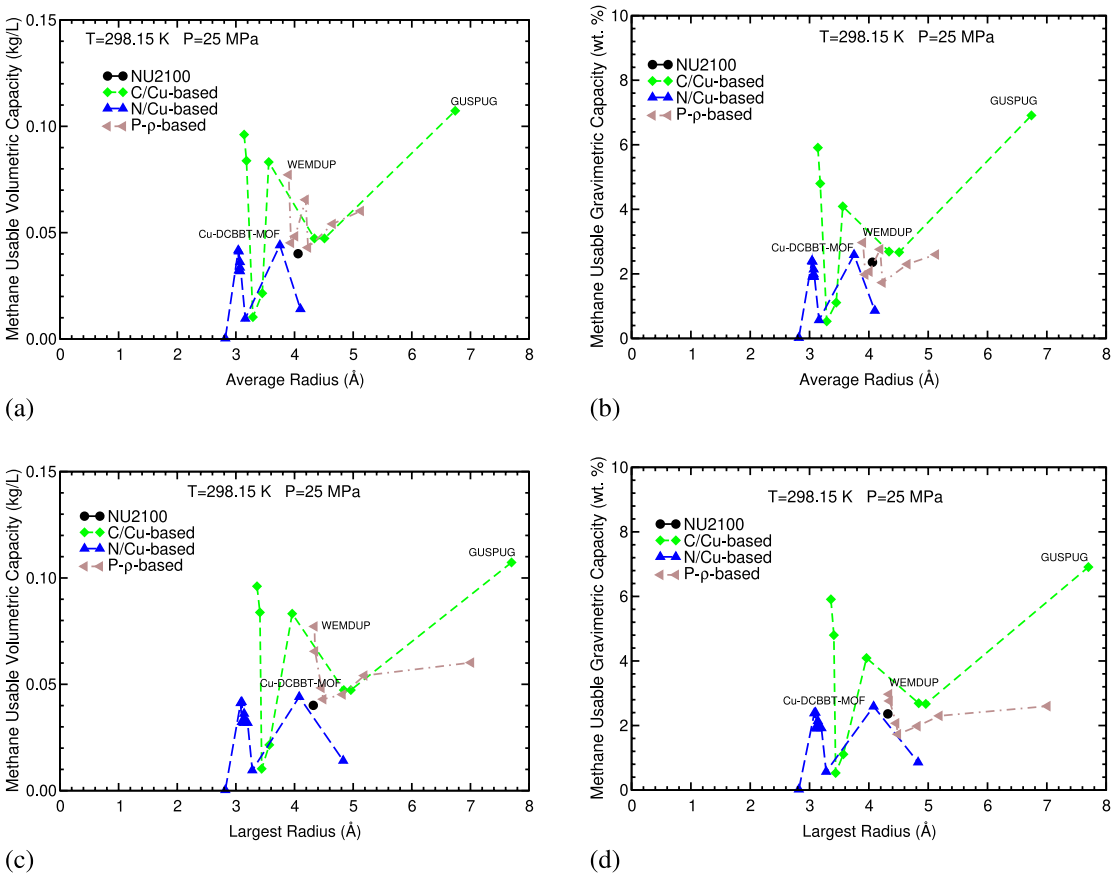

Fig. 13 Methane usable storage capacities at 25 MPa and 298.15 K vs average pore radius (panels (**a**) and (**b**)) and largest pore radius (panels (**c**) and (**d**)) for NU-2100, C/Cu, N/Cu and $P-\rho-$based MOFs.

The amount of space available and the intensity of the adsorbent-molecule interactions. That product is a balance between a purely geometric parameter, the porosity, and a parameter related with the physisorption interactions inside the pores of the materials. The methane capacities show a more clear dependence on that product (see the lower panels of Fig. 14): The capacities depend linearly on the product of porosity and isosteric heat. That dependence is approximate and can be used to design new MOFs that reach the DOE methane targets. According to the lower panels of Fig. 14, a MOF with a product equal or larger than 0.08 eV, would reach the DOE methane targets.

4.2 Dependence on the pressure

GCMC computational simulations were carried out in the range 0.5–35 MPa at 298.15 K, to assess the CH_4 capacities of NU-2100, alongside the most promising MOFs: GUSPUG, Cu-DCBBT-MOF and WEMDUP from the C/Cu, N/Cu and P-ρ-based MOFs, respectively. To provide a clearer comparison, a well-known and benchmark material, IRMOF-1, has also been included. The GCMC calculated isotherms are illustrated in Fig. 15. As far as we know, there are no experiments on methane storage at room temperature. Hence, the results in Fig. 15 are predictions of the methane isotherms of NU-2100 at room temperature.

IRMOF-1 performs better, in general, than NU-2100 in both total and usable volumetric capacities. Although IRMOF-1 has higher hydrogen and methane capacities than NU-2100, it must be considered some of its disadvantages: IRMOF-1 is based on zinc, which has a low level of toxicity, and is not air and moisture stable [130]. NU-2100 it is air and moisture stable.

The total methane isotherms of NU-2100, GUSPUG and WEMDUP are very similar for pressures equal or larger than 5 MPa. The total methane gravimetric isotherm of GUSPUG is higher than the gravimetric isotherms of NU-2100 and WEMDUP, because GUSPUG has a lower density than NU-2100 and WEMDUP and the density of NU-2100 and WEMDUP is similar. The total methane isotherms of Cu-DCBBT-MOF are lower than the isotherms of NU-2100, GUSPUG AND WEMDUP for pressures equal or larger than 3 MPa (see Fig. 15). The usable methane isotherms of GUSPUG, Cu-DCBBT-MOF and WEMDUP resemble the total isotherms. However, the usable isotherms of NU-2100 do not resemble the total isotherms of NU-2100. In fact,

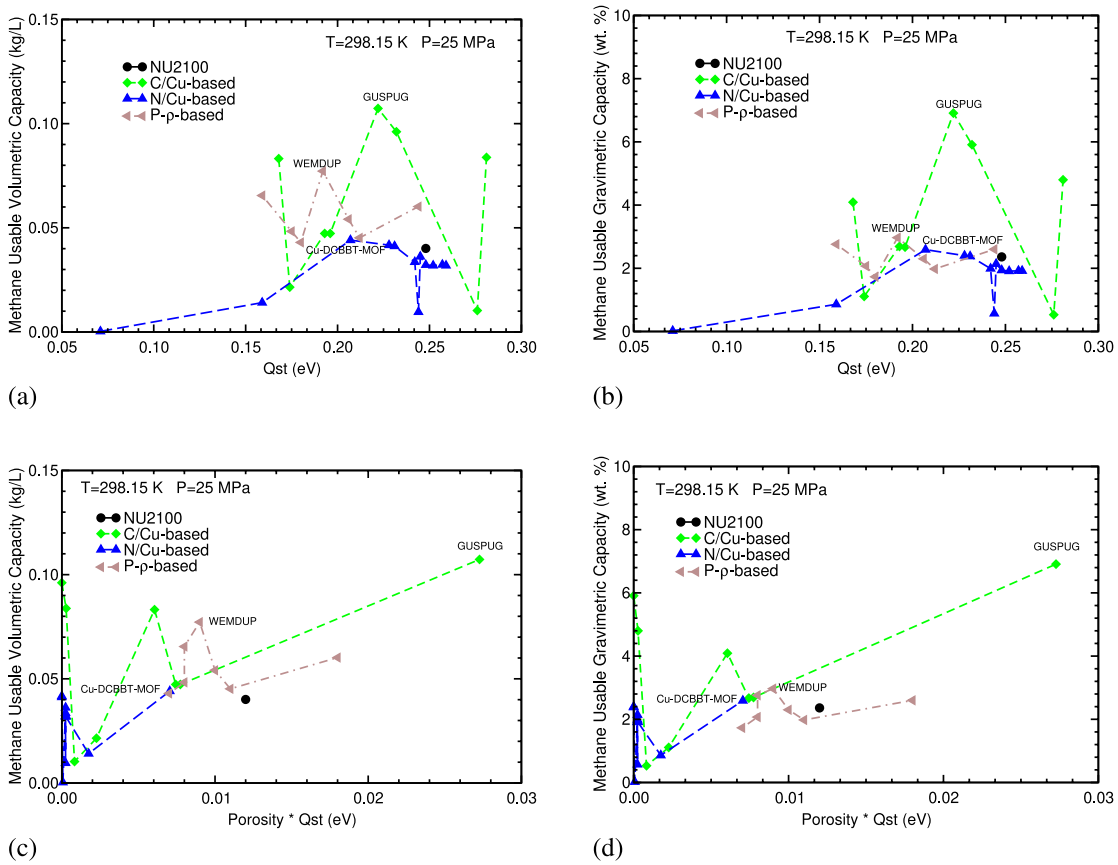

Fig. 14 Methane usable storage capacities at 25 MPa and 298.15 K vs the isosteric heat (panels (**a**) and (**b**)) and vs the product of the porosity and isosteric heat (panels (**c**) and (**d**)), for NU-2100, C/Cu, N/Cu and P-ρ-based MOFs.

the usable NU-2100 isotherms are similar to the usable Cu-DCBBT-MOF isotherms and two or three times lower than the usable isotherms of GUSPUG and WEMDUP (See Table S4 for the properties of the main MOFs).

To understand the origin of this different behaviour of the total and usable isotherms of NU-2100, the similarity of the usable isotherms of NU-2100 and Cu-DCBBT-MOF and the different behaviour of the isotherms of IRMOF-1, two properties or variables should be considered. First, this new material stores large amounts of methane at low pressures (0.1–0.5 MPa) and stores more methane at low pressures than the other MOFs (see Fig. 15). Second, the 3D interaction potential of NU-2100, Cu-DCBBT-MOF and IRMOF-1 has to be analyzed.

The 3D interaction potential energy in eV/molecule of a single methane molecule with NU-2100, Cu-DCBBT-MOF and IRMOF-1, obtained in the current GCMC simulations, are plotted in Fig. 16. The left panels in that figure show the interaction potential energies in the regions where the energies are equal or smaller than 0.1 eV and the right panels show $V(x, y, z)$ at the z planes (z = 12, 12 and 4 Å for NU-2100, Cu-DCBBT-MOF and IRMOF-1, respectively) where it reaches its lowest value. Those values are − 0.253, − 0.172 and − 0.122 eV/molecule for NU-2100, Cu-DCBBT-MOF and IRMOF-1, respectively. The channels or pores where the methane molecule interact strongly with the atoms of the MOFs are very similar in shape to those obtained for hydrogen (see Fig. 10). The interaction with methane is more intense than the interaction with the hydrogen molecule. This result is already known and is due to the fact that the methane molecule is larger than the hydrogen molecule.

The channels or pores available for methane in the NU-2100 and Cu-DCBBT-MOF are narrower compared to those for hydrogen (see Figs. 10 and 16). This helps explain why the isotherms of these two MOFs quickly reach an asymptotic value as pressure increases (see Fig. 15). This rapid saturation means that, although the total isotherms of NU-2100 and Cu-DCBBT-MOF are different, their usable isotherms are similar and low (lower than the usable isotherms of GUSPUG and WEMDUP). The channels for methane in IRMOF-1 are similar to those for hydrogen and are wider than the channels in NU-2100 and Cu-DCBBT-MOF, which explains that IRMOF-1 has higher methane capacities and that its isotherms saturate more slowly (see Fig. 15), in spite that the lowest value of $V(x, y, z)$ for

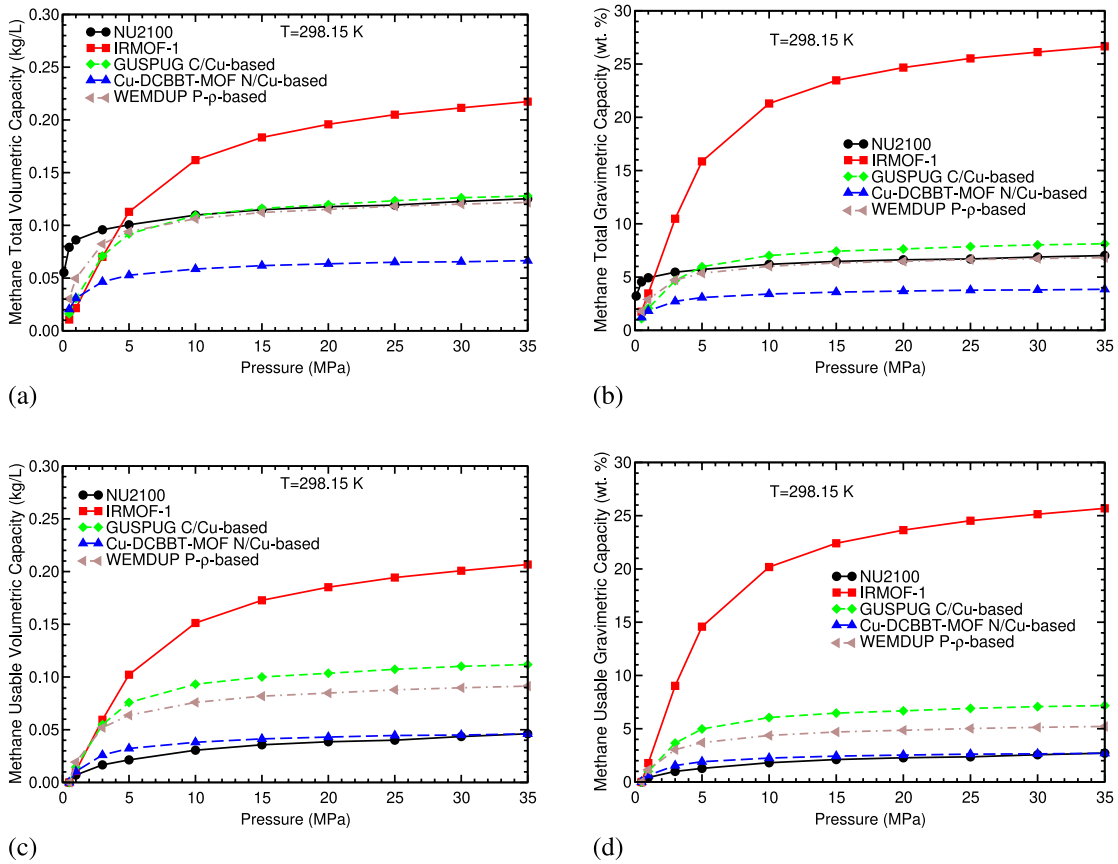

Fig. 15 Methane total (panels (**a**) and (**b**)) and usable (panels (**c**) and (**d**)) capacities at room temperature vs pressure for NU-2100 and best C/Cu, N/Cu, P-ρ-based MOFs and IRMOF-1.

IRMOF-1 is higher than the lowest values for the other MOFs.

4.3 Autonomy of the methane vehicle

The 2021 VW Golf GTI is a Compressed Natural Gas, CNG, vehicle. The deposits volume is 115 L and the fuel consumption is 100/4.3 km/kg [131]. The autonomy range is 248 miles (399 km). Let's suppose that NU-2100 is used as a solid porous adsorbent material inside the deposits and that the total volume is also 426 L, as in the hydrogen vehicle. The autonomy range of that methane vehicle, called ANG (Adsorbed Natural Gas) vehicle, as a function of the pressure is shown in Fig. 17. The autonomy range at pressure P is 426 L multiplied by the usable v_c(P) of NU-2100 and the fuel consumption of the 2021 VW Golf GTI. The autonomy range reaches the range of 400 km, the same autonomy as the 2021 VW Golf GTI, at 25 MPa.

We have also calculated and compared in Fig. 17 the autonomy of an ANG vehicle with the same volume and fuel consumption, using the total v_c's of activated carbon monoliths of the Ingevity Corporation [132, 133]. The data available cover the total v_c from 0.5 to 6.2 MPa. From those data, the usable v_c and the autonomy can be calculated. It can be noticed that a NU-2100 ANG vehicle would have about two times more autonomy.

5 Conclusions

The usable H_2 and CH_4 storage capacities of a novel Cu(I)-based MOF, NU-2100, recently synthesized by a Northwestern University group [99], at room temperature and pressures in the range 0.5–35 MPa were evaluated using GCMC simulations, with the LJ parameters [134–144] reported in Table S1 in the Supporting Information. The hydrogen and methane storage capacities of MOFs with similar C/Cu and N/Cu ratios, as well as MOFs with similar porosity-density-pore radii characteristics were also calculated using GCMC simulations.

There are experimental hydrogen total storage capacities at 273 and 296 K and up to 10 MPa. The hydrogen total storage capacities of NU-2100 obtained in the present GCMC simulations agree with the experimental storage capacities at 273 and 296 K. The differences between the experimental and theoretical capacities lie in the range 2–19%. The

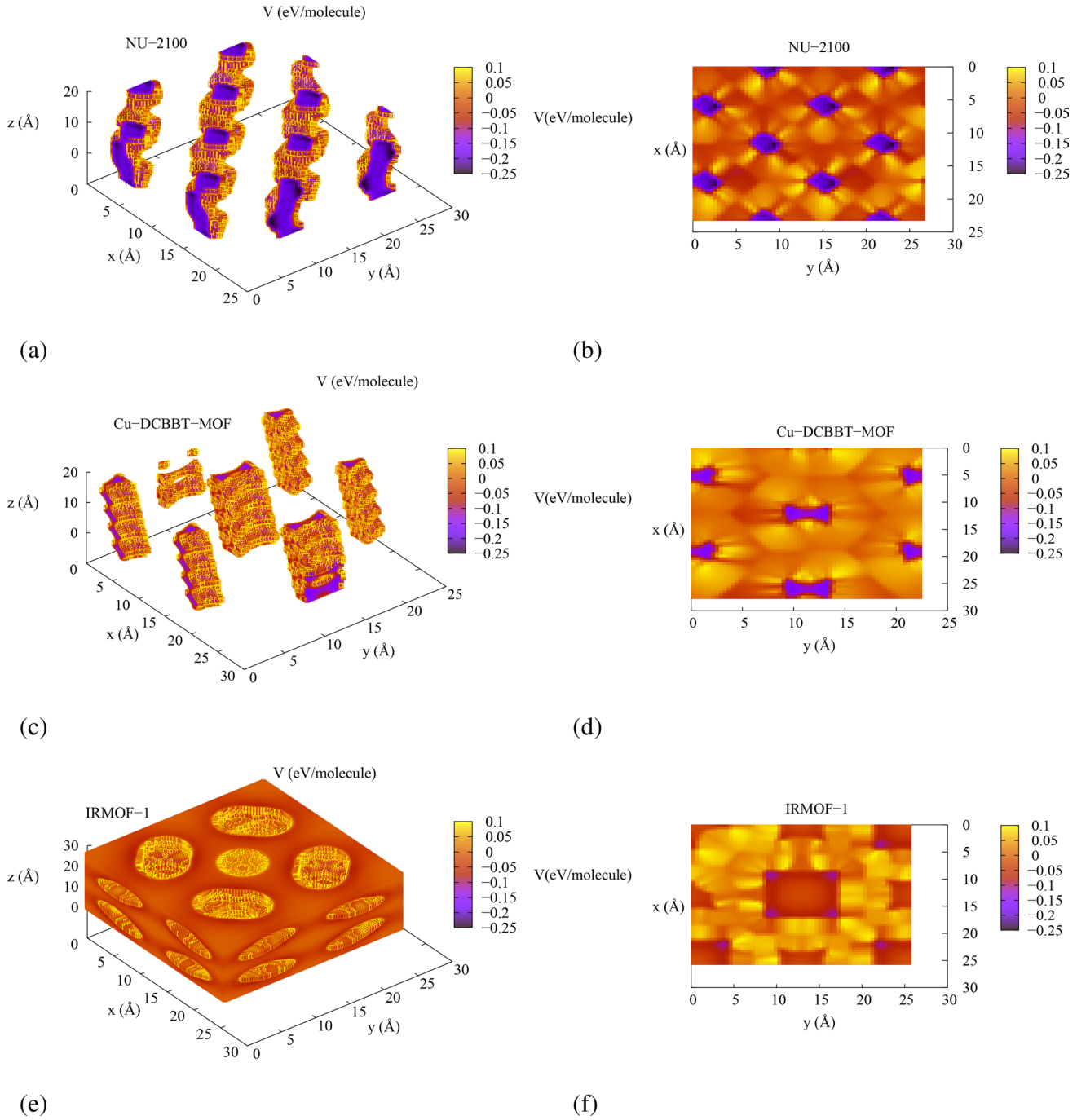

Fig. 16 Interaction potential energy in eV/molecule of a methane molecule with NU-2100 (panels (**a**) and (**b**)), Cu-DCBBT-MOF (panels (**c**) and (**d**)) and IRMOF-1 (panels (**e**) and (**f**)), obtained in the present GCMC simulations

present capacities at 298.15 K and 10–35 MPa are predictions for future experiments at those conditions.

The hydrogen storage capacities of NU-2100 exceed the capacities of the MOFs with similar C/Cu ratio, N/Cu ratio and porosity-density-pore size properties. NU-2100 has higher capacities because the H_2 molecules interact more strongly with the atoms of NU-2100.

IRMOF-1, one of the best benchmark or classical MOFs, has higher hydrogen and methane capacities than NU-2100. However, IRMOF-1 is a Zn-based MOF and Zn has a low level of toxicity and it is not air and moisture stable [130], while NU-2100 is air and moisture stable.

The total methane storage capacities of NU-2100 also are higher than those of MOFs with similar C/Cu ratio, N/Cu ratio and porosity-density-pore size properties. However,

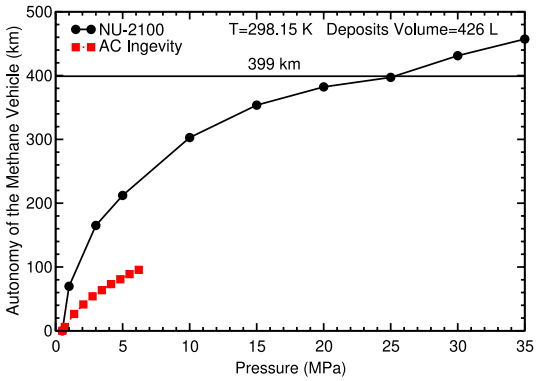

Fig. 17 Autonomy range of the methane vehicle with an adsorbed gas tank containing NU-2100 vs pressure of the tank at 298.15 K

the pores of this material are not wide enough to obtain high methane storage capacities. It is important to note that the methane storage capacities of NU-2100 obtained in the present simulations are predictions for future experiments.

Finally, the autonomy range of a hydrogen and methane vehicle that contains a tank with NU-2100 and stores the gas inside NU-2100 have been also calculated, based on the GCMC storage capacities. These vehicles could reach the autonomy range of vehicles that store the gas just by compression (Toyota 2024 and VW Golf GTI), but using a larger total volume tank and lower pressures. The use of lower pressures implies lower costs. Another advantage to consider is that NU-2100 shows air-stability, compared to other Cu(I) and Zn-based MOFs.

Supplementary Information The online version contains supplementary material available at https://doi.org/10.1007/s10450-025-00641-4.

Acknowledgements This study was supported by funding from the Spanish MICINN and Junta de Castilla y León, Grants PGC2018-093745-B-I00 and VA124G18, respectively. The use of the computer facilities at the Scientific Park of the University of Valladolid is also acknowledged.

Author contributions All authors whose names appear on the submission (1) made substantial contributions to the conception or design of the work; or the acquisition, analysis, or interpretation of data; or the creation of new software used in the work; (2) drafted the work or revised it critically for important intellectual content; (3) approved the version to be published; and (4) agree to be accountable for all aspects of the work in ensuring that questions related to the accuracy or integrity of any part of the work are appropriately investigated and resolved.

Funding Open access funding provided by FEDER European Funds and the Junta de Castilla y León under the Research and Innovation Strategy for Smart Specialization (RIS3) of Castilla y León 2021-2027.

Data Availability No datasets were generated or analysed during the current study.

Declarations

Competing interests The authors declare no competing interests.

References

1. Zhang, L., Jia, C., Bai, F., Wang, W., An, S., Zhao, K., Li, Z., Li, J., Sun, H.: A comprehensive review of the promising clean energy carrier: Hydrogen production, transportation, storage, and utilization (HPTSU) technologies. Fuel **355**, 129455 (2024). https://doi.org/10.1016/j.fuel.2023.129455
2. Chakraborty, S., Dash, S.K., Elavarasan, R.M., Kaur, A., Elangovan, D., Meraj, S.T., Kasinathan, P., Said, Z.: Hydrogen energy as future of sustainable mobility. Front. Energy Res. **10**, 893475 (2022). https://doi.org/10.3389/fenrg.2022.893475
3. Schlichtenmayer, M., Hirscher, M.: The usable capacity of porous materials for hydrogen storage. Appl. Physics A **122**, 379 (2016). https://doi.org/10.1007/s00339-016-9864-6
4. Jena, P.: Materials for hydrogen storage: Past, present, and future. J. Phys. Chem. Lett. **2**(3), 206–211 (2011). https://doi.org/10.1021/jz1015372
5. European Environment Agency, Transport and mobility. https://www.eea.europa.eu/en/topics/in-depth/transport-and-mobility (2024). Accessed 21 April 2025
6. Net Zero by 2050. A Roadmap for the Global Energy Sector. https://www.iea.org/reports/net-zero-by-2050 (2021). Accessed 21 April 2025
7. The long-term strategy of the United States, pathways to net-zero greenhouse gas emissions by 2050. https://unfccc.int/sites/default/files/resource/US-LongTermStrategy-2021.pdf (2021). Accessed 21 April 2025
8. Sdanghi, G., Maranzana, G., Celzard, A., Fierro, V.: Towards non-mechanical hybrid hydrogen compression for decentralized hydrogen facilities. Energies **13**(12), 3145 (2020). https://doi.org/10.3390/en13123145
9. Office of Energy Efficiency & Renewable Energy, Fuel Cell Technologies Office, DOE technical targets for onboard hydrogen storage for light-duty vehicles. https://www.energy.gov/eere/fuelcells/doe-technical-targets-onboard-hydrogen-storage-light-duty-vehicles (2018). Accessed 21 April 2025
10. Chu, C., Wu, K., Luo, B., Cao, Q., Zhang, H.: Hydrogen storage by liquid organic hydrogen carriers: Catalyst, renewable carrier, and technology—A review. Carbon Resour. Convers. **6**(4), 334–351 (2023). https://doi.org/10.1016/j.crcon.2023.03.007
11. Broom, D.P., Webb, C.J., Webb, K.E., Parilla, P.A., Gennett, T., Brown, C.M., Zacharia, R., Tylianakis, E., Klontzas, E., Froudakis, G.E., Steriotis, T.A., Trikalitis, P.N., Anton, D.L., Hardy, B., Tamburello, D., Corgnale, C., van Hassel, B.A., Cossement, D., Chahine, R., Hirscher, M.: Outlook and challenges for hydrogen

storage in nanoporous materials. Appl. Physics A **122**, 151 (2021). https://doi.org/10.1007/s00339-016-9651-4
12. Breeze, P.: Hydrogen energy storage. In: Power system energy storage technologies, ch 8, pp. 69–77. Elsevier, London (2018)
13. Hwang, H.T., Varma, A.: Hydrogen storage for fuel cell vehicles. Curr. Opin. Chem. Eng. **5**, 42–48 (2014). https://doi.org/10.1016/j.coche.2014.04.004
14. Ding, F., Yakobson, B.I.: Challenges in hydrogen adsorptions: from physisorption to chemisorption. Front. Phys. **6**, 142–150 (2011). https://doi.org/10.1007/s11467-011-0171-6
15. Assoualaye, G., Tom, A., Djongyang, N.: Monte Carlo study of hydrogen adsorption by MOF-5 doped with cobalt at ambient temperature and pressure. SN Appl. Sci. **2**, 1815 (2020). https://doi.org/10.1007/s42452-020-03627-9
16. Allendorf, M.D., Hulvey, Z., Gennett, T., Ahmed, A., Autrey, T., Camp, J., Cho, E.S., Furukawa, H., Haranczyk, M., Head-Gordon, M., Jeong, S., Karkamkar, A., Liu, D.-J., Long, J.R., Meihaus, K.R., Nayyar, I.H., Nazarov, R., Siegel, D.J., Stavila, V., Urban, J.J., Veccham, S.P., Wood, B.C.: An assessment of strategies for the development of solid-state adsorbents for vehicular hydrogen storage. Energy Environ. Sci. **11**, 2784–2812 (2018). https://doi.org/10.1039/C8EE01085D
17. Sherburne, M.: Natural gas could bridge gap from gasoline to electric vehicles, thanks to metal-organic frameworks. https://news.umich.edu/natural-gas-could-bridge-gap-from-gasoline-to-electric-vehicles-thanks-to-metal-organic-frameworks (2022). Accessed 21 April 2025
18. [CDATA[\text{CO}_2]]CO_2 emission performance standards for cars and vans. https://climate.ec.europa.eu/eu-action/transport/road-transport-reducing-co2-emissions-vehicles/co2-emission-performance-standards-cars-and-vans_en. Accessed 21 April 2025
19. Hren, R., Vujanović, A., Van Fan, Y., Klemeš, J.J., Krajnc, D., Čuček, L.: Hydrogen production, storage and transport for renewable energy and chemicals: An environmental footprint assessment. Renew. Sust. Energ. Rev. **173**, 113113 (2023). https://doi.org/10.1016/j.rser.2022.113113
20. Ogden, J., Jaffe, A.M., Scheitrum, D., McDonald, Z., Miller, M.: Natural gas as a bridge to hydrogen transportation fuel: Insights from the literature. Energy Policy **115**, 317–329 (2018). https://doi.org/10.1016/j.enpol.2017.12.049
21. Weger, L., Abánades, A., Butler, T.: Methane cracking as a bridge technology to the hydrogen economy. Int. J. Hydrogen Energy **42**(1), 720–731 (2017). https://doi.org/10.1016/j.ijhydene.2016.11.029
22. Sánchez-Bastardo, N., Schlögl, R., Ruland, H.: Methane pyrolysis for zero-emission hydrogen production: A potential bridge technology from fossil fuels to a renewable and sustainable hydrogen economy. Ind. Eng. Chem. Res. **60**(32), 11855–11881 (2021). https://doi.org/10.1021/acs.iecr.1c01679
23. Beckner, M., Dailly, A.: Adsorbed methane storage for vehicular applications. Appl. Energy **149**, 69–74 (2015). https://doi.org/10.1016/j.apenergy.2015.03.123
24. Yabing, H., Zhou, W., Guodong, Q., Chen, B.: Methane storage in metal-organic frameworks. Chem. Soc. Rev. **45**, 5657–5678 (2014)
25. Advanced Research Projects Agency - Energy, Department of Energy, Methane Opportunities for Vehicular Energy (MOVE) Program Overview. http://arpa-e.energy.gov/sites/default/files/documents/files/MOVE_ProgramOverview.pdf (2012). Accessed 21 April 2025
26. Advanced Research Projects Agency - Energy, Department of Energy, Methane Opportunities for Vehicular Energy (MOVE). https://arpa-e.energy.gov/technologies/programs/move (2012). Accessed 21 April 2025
27. International Organization for Standardization, ISO 15403-1:2006(en) Natural gas - Natural gas for use as a compressed fuel for vehicles - Part 1: Designation of the quality. https://www.iso.org/obp/ui/#iso:std:iso:15403:-1:ed-1:v1:en (2006). Accessed 21 April 2025
28. Office of Energy Efficiency & Renewable Energy, Hydrogen and Fuel Cell Technologies Office, High-Pressure Hydrogen Tank Testing. https://www.energy.gov/eere/fuelcells/high-pressure-hydrogen-tank-testing (2022). Accessed 21 April 2025
29. Yousaf, M., Ahmad, M., Zhao, Z.-P., Ishaq, T., Mahmood, N.: Current Trends in the Potential Use of the Metal-Organic Framework for Hydrogen Storage, Ch. 21, pp. 655–680. John Wiley & Sons Ltd. (2023). https://doi.org/10.1002/9781119829584.ch21
30. Granja-DelRío, A., Cabria, I.: Grand canonical Monte Carlo simulations of hydrogen and methane storage capacities of two novel Al-nia MOFs at room temperature. Int. J. Hydrogen Energy **50**, 685–696 (2024). https://doi.org/10.1016/j.ijhydene.2023.08.023
31. Cabria, I.: Grand Canonical Monte Carlo simulations of the hydrogen and methane storage capacities of novel but MOFs at room temperature. Int. J. Hydrogen Energy **50**, 160–177 (2024). https://doi.org/10.1016/j.ijhydene.2023.06.298
32. Caviedes, D., Cabria, I.: Grand canonical Monte Carlo simulations of the hydrogen storage capacities of slit-shaped pores, nanotubes and torusenes. Int. J. Hydrogen Energy **47**, 11916–11928 (2022). https://doi.org/10.1016/j.ijhydene.2022.01.229
33. Karki, S., Chakraborty, S.N.: A Monte Carlo simulation study of hydrogen adsorption in slit-shaped pores. Microporous Mesoporous Mater. **317**, 110970 (2021). https://doi.org/10.1016/j.micromeso.2021.110970
34. Cabria, I., Lebon, A., Torres, M.B., Gallego, L.J., Vega, A.: Hydrogen storage capacity of Li-decorated borophene and pristine graphene slit pores: a combined ab-initio and quantum-thermodynamic study. Appl. Surf. Sci. **562**, 150019 (2021). https://doi.org/10.1016/j.apsusc.2021.150019
35. Kessler, C., Eller, J., Gross, J., Hansen, N.: Adsorption of light gases in covalent organic frameworks: comparison of classical density functional theory and Grand Canonical Monte Carlo simulations. Microporous Mesoporous Mater. **324**, 111263 (2021). https://doi.org/10.1016/j.micromeso.2021.111263
36. Cabria, I.: Simulations of volumetric hydrogen storage capacities of nanoporous carbons: Effect of dispersion interactions as a function of pressure, temperature and pore width. Int. J. Hydrogen Energy **45**, 5697–5709 (2020). https://doi.org/10.1016/j.ijhydene.2019.03.071
37. Xu, W., Chen, Y., Song, M., Liu, X., Zhao, Y., Zhang, M., Zhang, C.: First-principles study on methane (CH_4) storage properties of graphdiyne. J. Phys. Chem. C **124**(15), 8110–8118 (2020). https://doi.org/10.1021/acs.jpcc.9b12009
38. Li, B., Wen, H.-M., Zhou, W., Xu, J.Q., Chen, B.: Porous metal-organic frameworks: Promising materials for methane storage. Chem **1**, 557–580 (2016). https://doi.org/10.1016/j.chempr.2016.09.009
39. Cheng, Y.-H., Zhang, C.-Y., Ren, J., Tong, K.-Y.: Hydrogen storage in Li-doped fullerene-intercalated hexagonal boron nitrogen layers. Front. Phys. **11**(5), 113101 (2016). https://doi.org/10.1007/s11467-016-0559-4
40. Blanco, A.A.G., Vallone, A.F., Korili, S.A., Gil, A., Sapag, K.: A comparative study of several microporous materials to store methane by adsorption. Microporous Mesoporous Mater. **224**, 323–331 (2016)
41. Hassani, A., Mosavian, H.M.T., Ahmadpour, A., Farhadian, N.: Hybrid molecular simulation of methane storage inside pillared graphene. J. Chem. Phys. **142**(23), 234704 (2015). https://doi.org/10.1063/1.4922541
42. Chouhan, R.K., Ulman, K., Narasimhan, S.: Graphene oxide as an optimal candidate material for methane storage. J. Chem. Phys. **143**(4), 044704 (2015). https://doi.org/10.1063/1.4927141

43. Peng, Y., Krungleviciute, V., Eryazici, I., Hupp, J.T., Farha, O.K., Yildirim, T.: Methane storage in metal-organic frameworks: Current records, surprise findings, and challenges. J. Am. Chem. Soc. **135**(32), 11887–11894 (2013). https://doi.org/10.1021/ja4045289
44. Zhou, X., Zhou, J., Sun, Q.: Tripyrrylmethane based 2D porous structure for hydrogen storage. Front. Phys. **6**, 220–223 (2011). https://doi.org/10.1007/s11467-011-0176-1
45. Li, S., Zhao, H.-M., Jena, P.: Ti-doped nano-porous graphene: A material for hydrogen storage and sensor. Front. Phys. **6**, 204–208 (2011). https://doi.org/10.1007/s11467-011-0178-z
46. Li, J., Furuta, T., Goto, H., Ohashi, T., Fujiwara, Y., Yip, S.: Theoretical evaluation of hydrogen storage capacity in pure carbon nanostructures. J. Chem. Phys. **119**(4), 2376–2385 (2003). https://doi.org/10.1063/1.1582831
47. Zhang, X., Liu, P., Zhang, Y.: The application of mofs for hydrogen storage. Inorganica Chim. Acta **557**, 121683 (2023). https://doi.org/10.1016/j.ica.2023.121683
48. Suh, M.P., Park, H.J., Prasad, T.K., Lim, D.-W.: Hydrogen storage in metal-organic frameworks. Chem. Rev. **112**(2), 782–835 (2012). https://doi.org/10.1021/cr200274s. (**pMID: 22191516**)
49. Li, A.: Metal-organic frameworks-based hydrogen storage strategies and applications. J. Phys: Conf. Ser. **2403**(1), 012022 (2022). https://doi.org/10.1088/1742-6596/2403/1/012022
50. Zhao, D., Wang, X., Yue, L., He, Y., Chen, B.: Porous metal-organic frameworks for hydrogen storage. Chem. Commun. **58**, 11059–11078 (2022). https://doi.org/10.1039/D2CC04036K
51. Demir, S., Altintas, C., Keskin, S., Topcu, Y.: Metal-organic frameworks for hydrogen storage. In: Gupta, R. (ed.) Handbook of Energy Materials, pp. 1–35. Springer Nature Singapore, Singapore (2022)
52. Zhang, B., Sun, Y., Xu, H., He, X.: Hydrogen storage mechanism of metal-organic framework materials based on metal centers and organic ligands. Carbon Neutraliz. **2**(6), 632–645 (2023). https://doi.org/10.1002/cnl2.91
53. Donà, L., Brandenburg, J.G., Civalleri, B.: Metal-organic frameworks properties from hybrid density functional approximations. J. Chem. Phys. **156**(9), 094706 (2022). https://doi.org/10.1063/5.0080359
54. Fanourgakis, G.S., Gkagkas, K., Froudakis, G.: Introducing artificial MOFs for improved machine learning predictions: Identification of top-performing materials for methane storage. J. Chem. Phys. **156**(5), 054103 (2022). https://doi.org/10.1063/5.0075994
55. Langmi, H.W., Ren, J., North, B., Mathe, M., Bessarabov, D.: Hydrogen storage in metal-organic frameworks: A review. Electrochim. Acta **128**, 368–392 (2014). https://doi.org/10.1016/j.electacta.2013.10.190
56. Collins, D.J., Zhou, H.-C.: Hydrogen storage in metal-organic frameworks. J. Mater. Chem. **17**, 3154–3160 (2007). https://doi.org/10.1039/B702858J
57. Alhasan, S., Carriveau, R., Ting, D.S.K.: A review of adsorbed natural gas storage technologies. Int. J. Environ. Stud. **73**, 343–356 (2016)
58. Liu, B., Wang, W., Wang, N., Au, C.T.: Preparation of activated carbon with high surface area for high-capacity methane storage. J. Energy Chem. **23**, 662–668 (2014)
59. Makal, T.A., Li, J.-R., Lu, W., Zhou, H.-C.: Methane storage in advanced porous materials. Chem. Soc. Rev. **41**, 7761–7779 (2012)
60. Lozano-Castelló, D., Cazorla-Amorós, D., Linares-Solano, A., Quinn, D.F.: Influence of pore size distribution on methane storage at relatively low pressure: preparation of activated carbon with optimum pore size. Carbon **40**, 989–1002 (2002)
61. Vasiliev, L.L., Kanonchik, L., Mishkinis, D.A., Rabetsky, M.I.: Adsorbed natural gas storage and transportation vessels. Int. J. Therm. Sci. **39**, 1047–1055 (2000)
62. Zhou, W., Wu, H., Hartman, M.R., Yildirim, T.: Hydrogen and methane adsorption in metal-organic frameworks: A high-pressure volumetric study. J. Phys. Chem. C **111**(44), 16131–16137 (2007). https://doi.org/10.1021/jp074889i
63. Vitillo, J.G., Regli, L., Chavan, S., Ricchiardi, G., Spoto, G., Dietzel, P.D.C., Bordiga, S., Zecchina, A.: Role of exposed metal sites in hydrogen storage in MOFs. J. Am. Chem. Soc. **130**(26), 8386–8396 (2008). https://doi.org/10.1021/ja8007159
64. García-Holley, P., Schweitzer, B., Islamoglu, T., Liu, Y., Lin, L., Rodriguez, S., Weston, M.H., Hupp, J.T., Gómez-Gualdrón, D.A., Yildirim, T., Farha, O.K.: Benchmark study of hydrogen storage in metal-organic frameworks under temperature and pressure swing conditions. ACS Energy Lett. **3**(3), 748–754 (2018). https://doi.org/10.1021/acsenergylett.8b00154
65. Denysenko, D., Grzywa, M., Jelic, J., Reuter, K., Volkmer, D.: Scorpionate-type coordination in MFU-4l metal-organic frameworks: Small-molecule binding and activation upon the thermally activated formation of open metal sites. Angew. Chem. Int. Ed. **53**(23), 5832–5836 (2014). https://doi.org/10.1002/anie.201310004
66. Jaramillo, D.E., Jiang, H.Z.H., Evans, H.A., Chakraborty, R., Furukawa, H., Brown, C.M., Head-Gordon, M., Long, J.R.: Ambient-temperature hydrogen storage via vanadium(II)-dihydrogen complexation in a metal-organic framework. J. Am. Chem. Soc. **143**(16), 6248–6256 (2021). https://doi.org/10.1021/jacs.1c01883
67. Chen, Z., Mian, M.R., Lee, S.-J., Chen, H., Zhang, X., Kirlikovali, K.O., Shulda, S., Melix, P., Rosen, A.S., Parilla, P.A., Gennett, T., Snurr, R.Q., Islamoglu, T., Yildirim, T., Farha, O.K.: Fine-tuning a robust metal-organic framework toward enhanced clean energy gas storage. J. Am. Chem. Soc. **143**(45), 18838–18843 (2021). https://doi.org/10.1021/jacs.1c08749
68. Jose, R., Bangar, G., Pal, S., Rajaraman, G.: Role of molecular modelling in the development of metal-organic framework for gas adsorption applications. J. Chem. Sci. **135**(2), 19 (2023). https://doi.org/10.1007/s12039-022-02130-5
69. Nath, K., Ahmed, A., Siegel, D.J., Matzger, A.J.: Computational identification and experimental demonstration of high-performance methane sorbents. Angew. Chem. Int. Ed. **61**(25), e202203575 (2022). https://doi.org/10.1002/anie.202203575
70. Forrest, K.A., Verma, G., Ye, Y., Ren, J., Ma, S., Pham, T., Space, B.: Methane storage in flexible and dynamical metal-organic frameworks. Chem. Phys. Rev. **3**(2), 021308 (2022). https://doi.org/10.1063/5.0072805
71. Suresh, K., Aulakh, D., Purewal, J., Siegel, D.J., Veenstra, M., Matzger, A.J.: Optimizing hydrogen storage in MOFs through engineering of crystal morphology and control of crystal size. J. Am. Chem. Soc. **143**(28), 10727–10734 (2021). https://doi.org/10.1021/jacs.1c04926
72. Zhang, X., Lin, R.-B., Wang, J., Wang, B., Liang, B., Yildirim, T., Zhang, J., Zhou, W., Chen, B.: Optimization of the pore structures of MOFs for record high hydrogen volumetric working capacity. Adv. Mater. **32**(17), 1907995 (2020). https://doi.org/10.1002/adma.201907995
73. Broom, D.P., Webb, C.J., Fanourgakis, G.S., Froudakis, G.E., Trikalitis, P.N., Hirscher, M.: Concepts for improving hydrogen storage in nanoporous materials. Int. J. Hydrogen Energy **44**(15), 7768–7779 (2019). https://doi.org/10.1016/j.ijhydene.2019.01.224
74. Kim, J., Yeo, S., Jeon, J.-D., Kwak, S.-Y.: Enhancement of hydrogen storage capacity and hydrostability of metal-organic frameworks (MOFs) with surface-loaded platinum nanoparticles and carbon black. Microporous Mesoporous Mater. **202**, 8–15 (2015). https://doi.org/10.1016/j.micromeso.2014.09.025
75. Rydén, J., Öberg, S., Heggie, M., Rayson, M., Briddon, P.: Hydrogen storage in the manganese containing metal-organic

framework MOF-73. Microporous Mesoporous Mater. **165**, 205–209 (2013). https://doi.org/10.1016/j.micromeso.2012.08.024
76. Hirscher, M., Panella, B., Schmitz, B.: Metal-organic frameworks for hydrogen storage. Microporous Mesoporous Mater. **129**(3), 335–339 (2010). https://doi.org/10.1016/j.micromeso.2009.06.005
77. Fei, S., Alizadeh, A., Hsu, W.-L., Delaunay, J.-J., Daiguji, H.: Analysis of the water adsorption mechanism in metal-organic framework MIL-101(Cr) by molecular simulations. J. Phys. Chem. C **125**(48), 26755–26769 (2021). https://doi.org/10.1021/acs.jpcc.1c06917
78. Hu, X., Wang, J., Li, S., Hu, X., Ye, R., Zhou, L., Li, P., Chen, C.: Pd-doped HKUST-1 MOFs for enhanced hydrogen storage: effect of hydrogen spillover. RSC Adv. **13**, 14980–14990 (2023). https://doi.org/10.1039/D3RA01788E
79. Park, J., Adhikary, A., Moon, H.R.: Progress in the development of flexible metal-organic frameworks for hydrogen storage and selective separation of its isotopes. Coord. Chem. Rev. **497**, 215402 (2023). https://doi.org/10.1016/j.ccr.2023.215402
80. Sengupta, D., Melix, P., Bose, S., Duncan, J., Wang, X., Mian, M.R., Kirlikovali, K.O., Joodaki, F., Islamoglu, T., Yildirim, T., Snurr, R.Q., Farha, O.K.: Air-stable Cu(I) metal-organic framework for hydrogen storage. J. Am. Chem. Soc. **145**(37), 20492–20502 (2023). https://doi.org/10.1021/jacs.3c06393
81. Zhang, X., Zheng, Q.-R., He, H.-Z.: Synergistic effect of hydrogen spillover and nano-confined AlH_3 on room temperature hydrogen storage in MOFs: By GCMC, DFT and experiments. Int. J. Hydrogen Energy **72**, 1224–1235 (2024). https://doi.org/10.1016/j.ijhydene.2023.05.227
82. Li, F.-G., Liu, C., Yuan, D., Dai, F., Wang, R., Wang, Z., Lu, X., Sun, D.: Ultrahigh hydrogen uptake in an interpenetrated Zn_4O-based metal-organic framework. CCS Chem **4**(3), 832–837 (2022). https://doi.org/10.31635/ccschem.021.202000738
83. Peedikakkal, A.M.P., Aljundi, I.H.: Upgrading the hydrogen storage of MOF-5 by post-synthetic exchange with divalent metal ions. Appl. Sci. **11**(24), 11687 (2021). https://doi.org/10.3390/app112411687
84. Mason, J.A., Oktawiec, J., Taylor, M.K., Hudson, M.R., Rodriguez, J., Bachman, J.E., Gonzalez, M.I., Cervellino, A., Guagliardi, A., Brown, C.M., Llewellyn, P.L., Masciocchi, N., Long, J.R.: Methane storage in flexible metal-organic frameworks with intrinsic thermal management. Nature **527**, 357–361 (2015). https://doi.org/10.1038/nature15732
85. Zhang, G., Liang, Y., Cui, G., Dou, B., Lu, W., Yang, Q., Yan, X.: Grand Canonical Monte Carlo simulation of the adsorption and separation of carbon dioxide and methane using functionalized Mg-MOF-74. Energy Rep. **9**, 2852–2860 (2023). https://doi.org/10.1016/j.egyr.2023.01.121
86. Yu, Y., Shang, M., Kong, L., Wang, L., Sun, T.: Influence of ligands within Al-based metal-organic frameworks for selective separation of methane from unconventional natural gas. Chemosphere **321**, 138160 (2023). https://doi.org/10.1016/j.egyr.2023.01.121
87. Singh, M., Shukla, A., Chakraborty, B.: Highly efficient hydrogen storage of a Sc decorated biphenylene monolayer near ambient temperature: ab initio simulations, Sustain. Energy Fuels **7**, 996–1010 (2023). https://doi.org/10.1039/D2SE01351G
88. Yeh, C.-H., Khan, A.H., Miyazak, T., Jiang, J.-C.: The investigation of methane storage at the Ni-MOF-74 material: a periodic DFT calculation. Phys. Chem. Chem. Phys. **23**, 12270–12279 (2021). https://doi.org/10.1039/D1CP01276B
89. Li, D.-Z., Chen, L., Liu, G., Yuan, Z.-Y., Li, B.-F., Zhang, X., Wei, J.-Q.: Porous metal-organic frameworks for methane storage and capture: status and challenges. New Carbon Mater. **36**(3), 468–496 (2021). https://doi.org/10.1016/S1872-5805(21)60034-3
90. Rosen, A.S., Notestein, J.M., Snurr, R.Q.: Structure-activity relationships that identify metal-organic framework catalysts for methane activation. ACS Catal. **9**(4), 3576–3587 (2019). https://doi.org/10.1021/acscatal.8b05178
91. Tsivion, E., Mason, J.A., Gonzalez, M.I., Long, J.R., Head-Gordon, M.: A computational study of CH_4 storage in porous framework materials with metalated linkers: connecting the atomistic character of CH_4 binding sites to usable capacity. Chem. Sci. **7**, 4503–4518 (2016). https://doi.org/10.1039/C6SC00529B
92. Sur, M., Dornfeld, M., Ganz, E.: Calculation of hydrogen storage capacity of metal-organic and covalent-organic frameworks by spillover. J. Chem. Phys. **131**(17), 174703 (2009). https://doi.org/10.1063/1.3257737
93. Samanta, A., Furuta, T., Li, J.: Theoretical assessment of the elastic constants and hydrogen storage capacity of some metal-organic framework materials. J. Chem. Phys. **125**(8), 084714 (2006). https://doi.org/10.1063/1.2337287
94. Sagara, T., Ortony, J., Ganz, E.: New isoreticular metal-organic framework materials for high hydrogen storage capacity. J. Chem. Phys. **123**(21), 214707 (2005). https://doi.org/10.1063/1.2133734
95. Sagara, T., Klassen, J., Ganz, E.: Computational study of hydrogen binding by metal-organic framework-5. J. Chem. Phys. **121**(24), 12543–12547 (2004). https://doi.org/10.1063/1.1809608
96. Ahmed, A., Seth, S., Purewal, J., Wong-Foy, A.G., Veenstra, M., Matzger, A.J., Siegel, D.J.: Exceptional hydrogen storage achieved by screening nearly half a million metal-organic frameworks. Nat. Commun. **10**, 1568 (2019). https://doi.org/10.1038/s41467-019-09365-w
97. Fu, J., Tian, Y., Wu, J.: Seeking metal-organic frameworks for methane storage in natural gas vehicles. Adsorption **21**, 499–507 (2015). https://doi.org/10.1007/s10450-015-9688-2
98. Basdogan, Y., Keskin, S.: Simulation and modelling of MOFs for hydrogen storage. CrystEngComm **17**, 261–275 (2015). https://doi.org/10.1039/C4CE01711K
99. Sengupta, D., Melix, P., Bose, S., Duncan, J., Wang, X., Mian, M.R., Kirlikovali, K.O., Joodaki, F., Islamoglu, T., Yildirim, T., Snurr, R.Q., Farha, O.K.: Air-stable Cu(I) metal-organic framework for hydrogen storage. J. Am. Chem. Soc. **145**(37), 20492–20502 (2023). https://doi.org/10.1021/jacs.3c06393
100. Metropolis, N.: The Beginning of the Monte Carlo Method. Los Alamos Science **15**, 125–130 (1987)
101. Cabria, I.: A fortran code to perform Grand Canonical Monte Carlo simulations of the gas storage capacities of solid materials. https://github.com/ivancabria/mcmgs/tree/master (Last Upload June 4, 2025)
102. Granja-DelRío, A., Cabria, I.: Exploring the hydrogen and methane storage capacities of novel DUT MOFs at room temperature: A grand canonical Monte Carlo simulation study. Int. J. Hydrogen Energy **54**, 665–677 (2024). https://doi.org/10.1016/j.ijhydene.2023.11.258
103. Soave, G.: Equilibrium constants from a modified Redlich-Kwong equation of state. Chem. Eng. Sci. **27**, 1197–1203 (1972). https://doi.org/10.1016/0009-2509(72)80096-4
104. Zhou, L., Zhou, Y.: Determination of compressibility factor and fugacity coefficient of hydrogen in studies of adsorptive storage. Int. J. Hydrogen Energy **26**, 597–601 (2001)
105. Xu, X.-H., Duan, Y.-Y., Yang, Z.: Crossover volume translation Soave-Redlich-Kwong equation of state for fluids. Ind. Eng. Chem. Res. **51**, 6580–6585 (2012)
106. Lennard-Jones, J.E.: On the determination of molecular fields. Proc. Roy. Soc. (London) A **106**, 463–477 (1924). https://doi.org/10.1098/rspa.1924.0082

107. Mayo, S.L., Olafson, B.D., Goddard, W.A., III.: DREIDING: A generic force field. J. Phys. C: Solid State Phys. **94**, 8897–8909 (1990)
108. Darkrim, F., Levesque, D.: Monte Carlo simulations of hydrogen adsorption in single-walled carbon nanotubes. J. Chem. Phys. **109**, 4981–4984 (1998)
109. The Siepmann Group, University of Minnesota, Transferable Potentials for Phase Equilibria. TraPPE-United Atom. http://trappe.oit.umn.edu/#UA. Accessed 21 April 2025
110. Feynman, R.P., Hibbs, A.: Quantum Mechanics and Path Integrals. McGraw-Hill, New York (1965)
111. Granja-DelRío, A., Cabria, I.: Insights into hydrogen and methane storage capacities: Grand Canonical Monte Carlo simulations of SIGSUA. J. Chem. Phys. **2024**, 154712 (2024). https://doi.org/10.1063/5.0193291
112. Cambridge Crystallographic Database Centre, CCDC, Structural chemistry data, software, and insights. https://www.ccdc.cam.ac.uk. Accessed 21 April 2025
113. Li, A., Bueno, R., Wiggin, S., Ward, S.C., Wood, P.A., Fairen-Jimenez, D.: The launch of a freely accessible MOF CIF collection from the CSD. Matter **4**, 1090–1106 (2021). https://doi.org/10.1016/j.matt.2021.03.006
114. Turner, P. J.: Grace Development Team, Grace: a WYSIWYG 2D plotting tool. http://plasma-gate.weizmann.ac.il/Grace, last version: 5.1.25 (2015). Accessed 21 April 2025
115. López, M., Torres, M.B., Cabria, I.: Grand canonical monte carlo simulations of the hydrogen storage capacities of zeolite-templated carbon schwarzites at room temperature. Int. J. Hydrogen Energy **71**, 1363–1372 (2024). https://doi.org/10.1016/j.ijhydene.2024.05.256
116. Yang, H., Li, L., Wu, J., Hou, H., Xiao, B., Fan, Y.: 3d coordination framework with uncommon two-fold interpenetrated $3^3 \cdot 5^9 \cdot 6^3$-lcy net and coordinated anion exchange. Chem. Eur. J. **15**, 4049–4056 (2009). https://doi.org/10.1002/chem.200802515
117. Yang, H., Li, L., Wu, J., Hou, H., Xiao, B., Fan, Y.: CCDC 703669: Experimental Crystal Structure Determination (2009). https://doi.org/10.5517/ccrm70l
118. Su, X., Zhong, Z., Yan, X., Xu, Y., Zhang, T., Ma, Y., Chen, L.: De novo design and facile synthesis of highly crystalline 2d conductive metal-organic frameworks: A "rotor-stator" strategy. J. Am. Chem. Soc. **146**, 9036–9044 (2024). https://doi.org/10.1021/jacs.3c13985
119. Su, X., Zhong, Z., Yan, X., Xu, Y., Zhang, T., Ma, Y., Chen, L.: CCDC 2306859: Experimental Crystal Structure Determination (2024). https://doi.org/10.5517/ccdc.csd.cc2hfgt7
120. Wu, D., Zhang, Z., Chen, X., Meng, L., Li, C., Li, G., Chen, X., Shi, Z., Feng, S.: A non-luminescent Eu-MOF-based "turn-on" sensor towards an anthrax biomarker through single-crystal to single-crystal phase transition. Chem. Commun. **55**, 14918–14921 (2019). https://doi.org/10.1039/C9CC08206A
121. Toyota Motor, 2024 Toyota Mirai. https://pressroom.toyota.com/vehicle/2024-toyota-mirai (2024). Accessed 21 April 2025
122. Andraos, E., Merino, G., Ritter, M.: Eco-audit of mofs as h_2 storage materials for vehicle applications, using novel refueling model. McGill Sci. Undergrad. Res. J. **16**, 12–18 (2021)
123. Kapelewski, M.T., Runčevski, T., Tarver, J.D., Jiang, H.Z.H., Hurst, K.E., Parilla, P.A., Ayala, A., Gennett, T., FitzGerald, S.A., Brown, C.M., Long, J.R.: Record high hydrogen storage capacity in the metal-organic framework Ni_2(m-dobdc) at near-ambient temperatures. Chem. Mater. **30**, 8179–8189 (2018). https://doi.org/10.1021/acs.chemmater.8b03276
124. Wong-Ng, W., Kaduk, J. A., Wu, H., Suchomel, M.: CCDC 1494751: Experimental Crystal Structure Determination (2016). https://doi.org/10.5517/ccdc.csd.cc1m5dsz
125. Wong-Ng, W., Kaduk, J.A., Wu, H., Suchomel, M.: Synchrotron X-ray studies of metal-organic framework M_2(2,5-dihydroxyterephthalate), M = (Mn Co, Ni, Zn) (MF074). Powder Diffr. **27**, 256–262 (2012). https://doi.org/10.1017/S0885715612000863
126. Liu, Y.-Y., Grzywa, M., Weil, M., Volkmer, D.: $[Cu_4$[CDATA[_4]]OCl_6[CDATA[_6]](DABCO)$_2$[CDATA[_2]]] [CDATA[\cdot]]0.5DABCO [CDATA[\cdot]]4CH_3[CDATA[_3]]OH ("MFU-5"): Modular synthesis of a zeolite-like metal-organic framework constructed from tetrahedral Cu_4[CDATA[_4]]OCl_6[CDATA[_6]] secondary building units and linear organic linkers. J. Solid State Chem. **183**, 208–217 (2010). https://doi.org/10.1016/j.jssc.2009.10.026
127. Liu, Y.-Y., Grzywa, M., Weil, M., Volkmer, D.: CCDC 748777: Experimental Crystal Structure Determination (2010). https://doi.org/10.5517/cct4536
128. Wang, P., Fan, R.-Q., Liu, X.-R., Wang, L.-Y., Yang, Y.-L., Cao, W.-W., Yang, B., Hasi, W., Su, Q., Mu, Y.: Two-/three-dimensional open lanthanide-organic frameworks containing rigid/flexible dicarboxylate ligands: synthesis, crystal structure and photoluminescent properties. CrystEngComm **15**, 1931–1949 (2013). https://doi.org/10.1039/c3ce26684b
129. Wang, P., Fan, R.-Q., Liu, X.-R., Wang, L.-Y., Yang, Y.-L., Cao, W.-W., Yang, B., Hasi, W., Su, Q., Mu, Y.: CCDC 860922: Experimental Crystal Structure Determination (2013). https://doi.org/10.5517/ccxwvp9
130. Yuan, S., Feng, L., Wang, K., Pang, J., Bosch, M., Lollar, C., Sun, Y., Qin, J., Yang, X., Zhang, P., Wang, Q., Zou, L., Zhang, Y., Zhang, L., Fang, Y., Li, J., Zhou, H.-C.: Stable metal-organic frameworks: Design, synthesis, and applications. Adv. Mater. **30**, 1704303 (2018). https://doi.org/10.1002/adma.201704303
131. Autoevolution. https://www.autoevolution.com/news/examining-the-cng-powered-engine-of-the-2021-vw-golf-tgi-151831.html (2020). Accessed 21 April 2025
132. Ingevity Corporation, Nuchar® FuelSorb ^{TM} [CDATA[^\text{ TM }]]. Activated Carbon Monoliths for Adsorbed Natural Gas (ANG) Vehicles. https://www.ingevity.com/uploads/market-pdfs/ANG-for-Natural-Gas-Vehicles.pdf (2025)
133. Ingevity Corporation, Nuchar® FuelSorb ^{TM} [CDATA[^\text{ TM }]]. Adsorbed natural gas (ANG): a low-pressure, bi-fuel natural gas vehicle solution. https://www.ingevity.com/uploads/market-pdfs/ANG-light-duty-vehicles.pdf (2025)
134. Guan, P., Mckenzie, D.R., Pailthorpe, B.A.: MD simulations of Ag film growth using the Lennard-Jones potential. J. Phys. Condens. Matter **8**, 8753–8762 (1996)
135. Tu, Y., Xiu, P., Wan, R., Hu, J., Zhou, R., Fang, H.: Water-mediated signal multiplication with Y-shaped carbon nanotubes. Proc. Natl. Acad. Sci. U.S.A. **106**, 18120–18124 (2009)
136. Rappé, A.K., Casewit, C.J., Colwell, K.S., Goddard, W.A., III., Skiff, W.M.: UFF, a full periodic table force field for molecular mechanics and molecular dynamics simulations. J. Am. Chem. Soc. **114**, 10024–10035 (1992). https://doi.org/10.1021/ja00051a040
137. Jorgensen, W.L., Madura, J.D., Swenson, C.J.: Optimized intermolecular potential functions for liquid hydrocarbons. J. Am. Chem. Soc. **106**, 6638–6646 (1984)
138. Singer, K., Taylor, A., Singer, J.V.L.: Thermodynamic and structural properties of liquids modelled by '2-Lennard-Jones centres' pair potentials. Mol. Phys. **33**, 1757–1795 (1977). https://doi.org/10.1080/00268977700101451
139. Šebesta, F., Sláma, V., Melcr, J., Futera, Z., Burda, J.V.: Estimation of transition-metal empirical parameters for molecular mechanical force fields. J. Chem. Theory Comput. **12**, 3681–3688 (2016). https://doi.org/10.1021/acs.jctc.6b00416
140. Reif, M. M., Hünenberger, P. H.: Computation of methodology-independent single-ion solvation properties from molecular simulations. IV. Optimized Lennard-Jones interaction parameter sets

for the alkali and halide ions in water. J. Chem. Phys. **134**, 144104 (2011)
141. Rzepka, M., Lamp, P., de la Casa-Lillo, M.A.: Physisorption of hydrogen on microporous carbon nanotubes. J. Phys. Chem. B **102**, 10894–10898 (1998). https://doi.org/10.1021/jp9829602
142. Cheung, P.S.Y., Powles, J.G.: The properties of liquid nitrogen. Mol. Phys. **30**, 921–949 (1975)
143. Mardiyah, R.. U., Arkundato, A., Purwandari, Misto E.: Energy cohesive calculation for some pure metals using the Lennard-Jones potential in Lammps molecular dynamics. J. Phys: Conf. Ser. **1491**, 012020 (2020). https://doi.org/10.1088/1742-6596/1491/1/012020
144. Eddaoudi, M., Kim, J., Rosi, N., Vodak, D., Wachter, J., O'Keeffe, M., Yaghi, O.M.: Systematic design of pore size and functionality in isoreticular MOFs and their application in methane storage. Science **295**, 469–472 (2002). https://doi.org/10.1126/science.1067208